1 Title: Transient Impairment in Microglial Function Causes Sex-Specific Deficits in
2   Synaptic and Hippocampal Function in Mice Exposed to Early Adversity
3
4 Short title: Effects of Early Adversity on Synaptic Pruning and Hippocampal Function

5

6   Sahabuddin Ahmed[1#]
7   Baruh Polis[1#]
8   Sumit Jamwal[1]
9   Basavaraju G. Sanganahalli[2,3]
10   Zoe MacDowell Kaswan[1]
11   Rafiad Islam[1]
12   Dana Kim[1]
13   Christian Bowers[1]
14   Lauryn Giuliano[1]
15   Thomas Biederer[4]
16   Fahmeed Hyder[2,3]
17   Arie Kaffman[1*]
18
19 # These authors have made similar contributions to the paper

20 Affiliations

21 1. Department of Psychiatry, Yale University School of Medicine, 300 George Street, Suite
22   901, New Haven CT, 06511, USA.
23 2. Department of Radiology & Biomedical Imaging and Magnetic Resonance Research
24   Center, Yale University, New Haven, CT, 06520, USA.
25 3. Department of Biomedical Engineering, Yale University, New Haven, CT, 06519, USA.
26 4. Department of Neurology, Yale School of Medicine, 100 College Street, New Haven, CT
27   06510, USA.
28
29 * Corresponding author: Arie Kaffman, 300 George Street, Suite 901, New Haven CT, 06511,
30 USA. email: arie.kaffman@yale.edu, phone: 203-785-6657
31

32 Key words: Early life adversity, mice, microglia, astrocytes, synaptic pruning, limited bedding
33 and nesting, hippocampus
34

35 Word count: manuscript:7508, abstract: 284

36
37
38
39
40
41
42
43
44

45 **Abstract**

46   Abnormal development and function of the hippocampus are two of the most consistent findings
47   in humans and rodents exposed to early life adversity, with males often being more affected
48   than females. Using the limited bedding (LB) paradigm as a rodent model of early life adversity,
49   we found that male adolescent mice that had been exposed to LB exhibit significant deficits in
50   contextual fear conditioning and synaptic connectivity in the hippocampus, which are not
51   observed in females. This is linked to altered developmental refinement of connectivity, with LB
52   severely impairing microglial-mediated synaptic pruning in the hippocampus of male and female
53   pups on postnatal day 17 (P17), but not in adolescent P33 mice when levels of synaptic
54   engulfment by microglia are substantially lower. Since the hippocampus undergoes intense
55   synaptic pruning during the second and third weeks of life, we investigated whether microglia
56   are required for the synaptic and behavioral aberrations observed in adolescent LB mice.
57   Indeed, transient ablation of microglia from P13-21, in normally developing mice caused sex-
58   specific behavioral and synaptic abnormalities similar to those observed in adolescent LB mice.
59   Furthermore, chemogenetic activation of microglia during the same period reversed the
60   microglial-mediated phagocytic deficits at P17 and restored normal contextual fear conditioning
61   and synaptic connectivity in adolescent LB male mice. Our data support an additional
62   contribution of astrocytes in the sex-specific effects of LB, with increased expression of the
63   membrane receptor MEGF10 and enhanced synaptic engulfment in hippocampal astrocytes of
64   17-day-old LB females, but not in LB male littermates. This finding suggests a potential
65   compensatory mechanism that may explain the relative resilience of LB females. Collectively,
66   these studies highlight a novel role for glial cells in mediating sex-specific hippocampal deficits
67   in a mouse model of early-life adversity.
68
69
70
71
72
73
74
75
76
77
78
79
80
81
82
83
84
85
86
87
88
89
90
91
92
93
94

95 **INTRODUCTION**
96 Adverse childhood experiences, such as abuse, neglect, extreme poverty, and neighborhood
97 violence, can lead to abnormal brain development and early-life emotional and cognitive
98 challenges (Kaffman and Meaney, 2007; McLaughlin et al., 2020; Teicher and Samson, 2016).
99 Approximately half of all childhood psychopathologies are attributed to early life adversity (ELA)
100 (Green et al., 2010). In many cases, these early consequences persist into adulthood, resulting
101 in chronic psychiatric and medical conditions that are difficult to treat (Anda et al., 2006;
102 Kaffman and Meaney, 2007; Nemeroff, 2016). A better understanding of the underlying biology
103 is essential for diagnosing the structural and functional changes associated with ELA and for
104 developing more effective interventions.
105
106 Some of the most consistent findings in individuals exposed to ELA are reduced hippocampal
107 volume and abnormal hippocampal function (Crozier et al., 2014; De Bellis et al., 2013; Lambert
108 et al., 2019; Teicher and Samson, 2016), with some evidence indicating more pronounced
109 deficits in men than women (Garvin and Bolton, 2022; Teicher and Samson, 2016; White and
110 Kaffman, 2019). Rodents exposed to different models of ELA also exhibit abnormal
111 hippocampal function, with particularly pronounced deficits observed in mice reared with limited
112 bedding and nesting (LB) (Rocha et al., 2021). However, most of the studies to date have
113 focused on outcomes in adult LB males, with only a few examples examining this issue in both
114 sexes (Bath et al., 2017; Naninck et al., 2015; Rocha et al., 2021). Additionally, only two studies
115 have examined the effect of LB on hippocampal function and development in adolescent mice
116 (Bath et al., 2017; Islam et al., 2023), a period in which sex-specific effects of ELA appear to be
117 more prominent (Gershon et al., 2008; White and Kaffman, 2019).
118
119 Microglia, the immune innate cells in the brain, control the refinement of connectivity and play a
120 critical role in establishing sexually dimorphic processes during brain development (VanRyzin et
121 al., 2020). Microglia are also responsible for distinct physiological and behavioral responses in
122 adult males and females (Dorfman et al., 2017; Sorge et al., 2015; Villa et al., 2018; Yanguas-
123 Casás, 2020). Given the prominent role that microglia play in programing sex differences we
124 investigated whether abnormal microglial-mediated synaptic pruning during the second and third
125 weeks of life contributes to sex-specific deficits in synaptic function and contextual freezing
126 observed in adolescent LB mice. Microglia play a crucial role in eliminating nonfunctional
127 synapses during a critical period of development and disrupting this process leads to the
128 retention of a large number of weak synapses, reduced connectivity, and abnormal behavior
129 and cognition later in life (Bolton et al., 2022; Filipello et al., 2018; Johnson and Kaffman, 2017;
130 Zhan et al., 2014). Moreover, significant impairments in microglial-mediated synaptic pruning
131 occur in LB pups, as well as increased spine density that persists in adolescent mice (Bolton et
132 al., 2022; Dayananda et al., 2022). In this study, we determined that LB causes severe synaptic
133 and contextual fear conditioning deficits in adolescent male, but not female, littermates. These
134 deficits were accompanied by impairment in microglial-mediated phagocytic activity in 17-day-
135 old male and female pups when synaptic pruning peaks in the developing hippocampus
136 (Filipello et al., 2018; Scott-Hewitt et al., 2020; Zhan et al., 2014). Abnormal microglial
137 phagocytic activity did not persist into adolescence when phagocytic activity is eight-fold lower.
138 Furthermore, transient elimination of microglia during the second and third weeks of life induced
139 similar sex-specific deficits in synaptic function and contextual fear conditioning observed in LB
140 mice and chemogenetic activation of microglia during this critical period was sufficient to
141 normalize the synaptic and contextual deficits observed in adolescent LB male mice. Finally, we
142 found that LB female, but not LB male littermates are able to upregulate synaptic pruning in
143 astrocytes.
144
145 **METHODS**

146
147 *Animals*
148 BALB/cByj mice (Stock # 001026, Jackson Laboratories) were housed in standard Plexiglas
149 cages and kept on a standard 12:12 h light-dark cycle (lights on at 07.00 AM) with constant
150 temperature and humidity (22 °C and 50%) and food and water provided ad libitum.
151 CX3CR1^{creET2}-DTA mice (C57BL/6J background) were generated by crossing CX3CR1-Cre-ET2
152 mice (Jax 021160) and ROSA26-eGFP-DTA mice (Jax# 006331). CX3CR1 ^{creET2}-Gq-DREADD
153 mice (C57BL/6J background) were generated by crossing CX3CR1-Cre-ET2 mice (Jax 021160)
154 and CAG-LSL-Gq-DREADD mice (Jax# 026220). All studies were approved by the Institutional
155 Animal Care and Use Committee (IACUC) of Yale University and were conducted in accordance
156 with the recommendations of the NIH Guide for the Care and the Use of Laboratory Animals.
157
158 *Limited Bedding*
159 The limited bedding (LB) procedure was performed as described previously (Dayananda et al.,
160 2022; Johnson et al., 2018; White et al., 2020). Briefly, mice were mated at a 3:1 female to male
161 ratio, in standard mouse Plexiglas cages layered with 500 cc of corncob bedding but with no
162 nesting material. Visibly pregnant dams were transferred to maternity cages containing
163 500 cc corncob bedding but no nesting material. At birth, postnatal day (P0) litters were culled to
164 5-8 pups and randomized to either control (CTL) or LB conditions. Mice raised under CTL
165 condition were provided with 500 cc of fresh corncob bedding with an additional 15 cc of soiled
166 bedding from the original cage and one 5 × 5 cm nestlet per cage. LB litters were provided with
167 125 cc of corncob,15 cc of soiled bedding from the original cage, and no nesting material.
168 Bedding was changed weekly, and mice were weaned on P26 and housed with 2-3 individuals
169 of the same-sex and condition per cage.
170
171 *Contextual fear conditioning*
172 Contextual fear conditioning was performed using a Med Associates' fear conditioning chamber
173 as previously described (White et al., 2020).
174
175 Tissue collection
176 Tissues were collected between 11:00 and 13:00 to minimize the diurnal effects of
177 corticosterone. Mice were anesthetized and transcardially perfused with ice-cold PBS/heparin
178 (50 u/ml) solution (Bio-Rad, Cat #1610780; Sigma, Cat# H3393), followed by 10% formalin
179 (Polyscience, Cat# 08279-20). The brains were postfixed for 1hr with 10% formalin at r.t. and
180 then stored in PBS at 4°C until they were processed for immunohistochemistry or DiOlistic
181 labeling.
182
183 DiOlistic labeling
184 This procedure was performed as described previously (Forlano and Woolley, 2010) with the
185 following modifications. Perfused brains were coronally sectioned at 200 µm using a VT1000S
186 vibratome (Leica). Sections containing the dorsal hippocampus (Paxinos, Bregma -1.82 to -
187 2.30) were labeled with a Helios gene gun (Bio-Rad) using 200 psi and µm tungsten particles
188 coated with fluorescent 1,1'-Dioctadecyl-3,3,3',3'-Tetramethylindocarbocyanine Perchlorate (DiI,
189 Thermo Fisher Scientific; D-282). The DiI was allowed to diffuse at r.t. for 24 hrs and then
190 washed with PBS. The slices were then postfixed with 10% formalin for 2hrs at r.t, washed with
191 PBS, mounted on Superfrost Plus slides (Therrmo Scientific, Cat. # 4951F-001) with
192 Fluoromount-G^{TM} solution (Invitrogen, Cat. # 00-4958-02), and coverslipped.
193
194 Immunohistochemistry
195 Fifty-micron coronal sections were collected using a VT1000S vibratome (Leica) in 6 pools,
196 each containing 16-18 slices, spanning the entire rostral-caudal axis of the hippocampus. To

197 assess microglial phagocytic activity, one pool of slices was stained with rabbit anti-Iba1 (1:500;
198 Wako, Cat. #019-19741), mouse anti -PSD95 (1:100; Merck-Millipore, Cat. #MAB1596), and rat
199 anti -CD68 (1:400; Bio-Rad, Cat. # MCA1957T).To assess the density of functional
200 glutamatergic synapses, slice were incubated with guinea pig anti-Vglut2 (1:700; EMD-Millipore
201 Cat. #AB2251-I), and mouse anti-PSD95 (1:100; Merck-Millipore, Cat. #MAB1596). Astrocytic
202 phagocytic activity and MEGF10 levels were characterized using sequential staining in order to
203 minimize cross reactivity between mouse and rat antibodies. Briefly, sections were washed with
204 TBST (3 X 15 min each) and blocked with Triton-X 100 (0.5%) + normal goat serum (NGS) (5%)
205 for 2 hr. Sections were then first incubated with mouse anti-PSD95 antibodies (1:100; Merck-
206 Millipore, Cat. #MAB1596) overnight at 4°C, washed and incubated with Alexa Flour^{TM} 555 goat
207 anti-mouse secondary antibody (1:400; Invitrogen Cat. # A21422). The sections were again re-
208 blocked with 5% NGS for 2 hr (second serum blocking) and subsequently stained with rat anti-
209 GFAP (1:500; Invitrogen Cat. #13-0300), and rabbit anti-Megf10 (1: 400; EMD-Millipore Cat.
210 #ABC-10). Stained slices were then labelled with the appropriate fluorescently labeled
211 secondary antibodies (1:400; Thermo Fisher) and then mounted on glass slides with
212 VECTASHIELD HardSet antifade mounting medium with DAPI (Vector laboratories Cat#
213 10955).
214
215 Microscopy and image analysis
216 Spine density and morphology were assessed in fully impregnated CA1 pyramidal cells located
217 in the dorsal hippocampus and imaged with a Zeiss LSM 880 confocal workstation equipped
218 with Airyscan using 20X objective at 0.5 µm intervals. Secondary and tertiary apical dendrites
219 located in the stratum radiatum and were 20 ±3 µm in length and 1.0 ±0.2 µm in diameter were
220 then cropped and modeled using the semiautomated filament tracer tool in Imaris 10.0 (Oxford
221 Instruments). The default setting of the Classify Spines X Tension tool in Imaris was
222 subsequently used to classify spines as stubby, mushroom, long thin, or filopodia and to
223 calculate total spine density and maturity index= density of mushroom/all other spine categories.
224 The data from 6 dendrites were averaged to obtain the total spine density and maturity index for
225 each individual animal. Microglial volume, CD68 volume, and the number of PSD95 puncta
226 inside microglia located in the stratum radiatum were determined as described previously
227 (Dayananda et al., 2022). To assess glutamatergic spine density, high-resolution (1024 x 1024),
228 6-8 confocal Z stack images of the stratum radiatum were acquired using an Olympus FV-3000
229 microscope with a 60X objective, 2x digital zoom and 0.30 µm intervals for a total thickness of
230 15-20 µm. The acquired images were deconvoluted and processed using the Imaris version-
231 9.9.1 (Oxford Instruments) according to the following protocol. A 25 µm x 50 µm x10 µm region
232 of interest was selected using the cropped 3D function with each channel adjusted using
233 gaussian filter, automated background subtraction, and gamma correction. A 3D reconstruction
234 spots were created for each channel using the 'spot function' with an XY diameter of 0.2 µm and
235 Z-axis elongation at 10 µm. Spots were selected based on the 'Quality' filter type with the center
236 point and radius size set at 10. Finally, the spots which were in close proximity (0-250 µm apart)
237 were considered functional synapses and were calculated using the 'shortest distance to spot-
238 spot' filter. The densities obtained from 6-8 pictures were averaged to determine VGlut2,
239 PSD95, and glutamatergic synapse densities for each mouse. Z- stack images of GFAP-
240 positive cells localized in the stratum radiatum were acquired using an Olympus FV-3000 using
241 a 60x objective, 2x digital zoom, and 0.30 µm intervals for a total thickness of 20 µm and
242 processed using the 3D surface rendering function in Imaris. A 50 µm x 50 µm x 10 µm region
243 of interest was copped using the 3D function and each channel adjusted via a Gaussian filter
244 using automated background subtraction and gamma correction. GFAP and Megf10 surfaces
245 were created using a semiautomated thresholds of 0.3 µm and 0.2 µm respectively. PSD95
246 puncta were detected and quantified using the 'spot function' with a threshold of 0.2 µm. Finally,
247 the number of PSD95 puncta and Megf10 volume engulfed inside GFAP-positive cells were

248   quantified using the 'spot closed to surfaces' function with a threshold set at zero.
249   Measurements obtained from 5-6 astrocytes were averaged to determine cell volume, number
250   of PSD95 puncta per cell, and volume of MEGF10 staining per cell for each mouse.
251
252   Resting state fMRI (rsfMRI)
253   We used functional connectivity density (FCD) mapping to assess the local functional
254   connectivity. FCD is a voxel- and degree-based metric, which identifies the number of correlated
255   voxels to a base voxel without identifying the precise location of the correlated voxels. These
256   metrics are degree based, as they are based on the number of voxels that a given voxel is
257   strongly correlated with, or functionally ''connected to.'' Global FCD determination is a standard
258   graph theory-based analysis determining brain functional connectivity using resting state fMRI
259   and originally demonstrated in the human brain (Tomasi and Volkow, 2010). Local functional
260   connectivity was determined as described previously (Farina et al., 2021; Sanganahalli et al.,
261   2021). Mice were initially anesthetized with 2-3 % isoflurane, and a PE 50 tubing was placed
262   into the i.p. cavity for dexmedetomidine (sedative) infusion. Thereafter, mice were maintained
263   under complete anesthesia with 0.25% isoflurane and 250 µg/kg/h i.p, of dexmedetomidine.
264   Body temperature was maintained at 36°C–37°C using a heating pad and monitored using an
265   MRI-compatible rectal probe throughout the MRI experiments. Heart rate and respiratory rate
266   were continuously monitored throughout the MRI experiments. Dynamic blood oxygenation
267   dependent (BOLD) data were obtained using a Bruker 9.4T/16 magnet (Bruker BioSpin, MA,
268   USA) using a single-shot gradient echo, echo planar imaging (GE-EPI) sequence with the
269   following parameters: TR of 1000 ms, TE of 12 ms, in-plane resolution of 400 × 400 µm and
270   slice thickness of 1000 µm, for a total of 300 images for each run. BOLD time series across all
271   voxels were detrended using a second order fit and bandpass filtered (0.001 to 0.1 Hz) to
272   exclude slow drift of the signal. Images were then registered to a brain template (200 x 200 x
273   200 um spatial resolution) followed by spatial Gaussian filtering (FWHM=1.5 mm) as previously
274   described (Farina et al., 2021; Sanganahalli et al., 2021).
275
276   Transient microglial ablation
277   CX3CR1^{creET2}-DTA male breeders (C57BL/6J background) that were homozygous for the
278   CX3CR1-Cre-ET2 transgene (Jax #021160) and heterozygous for the floxed diphtheria toxin A
279   gene (R26-eGFP-DTA, (Jax #006331) were mated with Balb/cByj females to generate mixed
280   litters in which half of the pups were CX3CR1-$^{creET/WT}$;DTA$^{DTA/WT}$ (abbreviated as DTA) and the
281   other half are CX3CR1-$^{creET/WT}$;DTA$^{WT/WT}$ (abbreviated as WT). All litters were raised under CTL
282   conditions (i.e. 2 cups of bedding and one nestlet) and at P10 administered tamoxifen i.p. (30
283   mg/kg) to rapidly ablate microglia. Most pups were weaned at P26 and housed with 2-3 same-
284   sex mice until tested in the contextual fear conditioning at P30-33, although a few pups were
285   sacrificed at different ages to assess microglial elimination or were tested in the open field test
286   at P17. Twenty-four hours after testing contextual freezing, mice were perfused to assess spine
287   density and morphology or glutamatergic spine density. An additional cohort of P30-33 mice
288   were scanned to assess local functional connectivity using rsfMRI.
289
290   Transient chemogenetic activation of microglia
291   CX3CR1^{creET2}-Gq-DREADD male breeders (C57BL/6J background) that were homozygous for
292   the CX3CR1-Cre-ET2 transgene (Jax #021160) and heterozygous for the CAG-LSL-Gq-
293   DREADD transgene (Gq-DREADD, Jax# 026220) were mated with Balb/cByj females to
294   generate mixed litters in which half of the pups were CX3CR1-$^{creET/WT}$;Gq-DREADD$^{Gq/WT}$
295   (abbreviated as Gq) and the other half were CX3CR1-$^{creET/WT}$; Gq-DREADD$^{WT/WT}$ (abbreviated as
296   WT). Litters were randomized to CTL or LB conditions and administered tamoxifen i.p. (30
297   mg/kg, MP Biomedicals LLC Cat# 156738) at P10 to induce Gq-DREADD expression in
298   microglia. CNO (1 mg/kg, Sigma, Cat#C0832) was then administered i.p. daily on P13, P14,

299 P15, P16, and P17. Some pups were processed at P17, 1hr after the last CNO injection, to
300 assess in vivo phagocytic activity. All other mice were weaned at P26 and housed with 2-3
301 same-sex mice until tested in the contextual fear conditioning at P30-33. Twenty-four hours after
302 contextual fear conditioning, mice were perfused to assess spine density and morphology or
303 glutamatergic spine density.
304
305 Statistical analysis
306 The data were carefully screened for inaccuracies, outliers, normality, and homogeneity of
307 variance using SPSS (IBM Corp. version 26) and visualized with GraphPad Prism (iOS, version
308 10.0). Two-way ANOVA was used to assess the effects of rearing (CTL vs. LB), sex and their
309 interaction on contextual freezing, the maturity index, and glutamatergic synapse density (Fig 1),
310 as well as in vivo phagocytic activity and MEGF10 expression in astrocytes (Fig 6). Significant
311 main effect of rearing or interaction were followed by a preplanned Sidak-post-hoc analysis for
312 each sex. The effects of rearing (CTL vs LB), sex, age (P17 vs P33), and their interaction on
313 microglial-phagocytic activity (Fig 2) were initially examined using a 3-way ANOVA but simplified
314 to a two-way ANOVA focusing on the main effects of rearing and age and their interaction.
315 Significant interaction between rearing and age was followed by a preplanned Tukey-HSD post-
316 hoc comparison across all groups. For microglial ablation, a two-way ANOVA was used to
317 assess the effects of genotype (WT vs DTA), sex, and their interaction on contextual freezing,
318 the maturity index, and glutamatergic synapse density with significant main effects of genotype
319 or interaction followed by preplanned Sidak-post-hoc analyses for each sex. Three-way ANOVA
320 was initially used to assess the effects rearing (CTL vs LB), sex, and genotype (WT vs. Gq) on
321 microglial phagocytic activity in-vivo in P17 pups. However, since similar outcomes were seen in
322 males and females, this was simplified to a two-way ANOVA focusing on the effects of rearing
323 and genotype with significant interaction followed by Tukey-HSD post-hoc comparisons across
324 all groups (Fig 4). Three-way ANOVA was also used to assess the effects of rearing (CTL vs
325 LB), sex, and genotype (WT vs. Gq) on contextual freezing in P33 adolescent mice. However,
326 since there was a significant interaction between rearing and sex, we conducted separate two-
327 way analyses in males and females. Significant effects of rearing or interaction were followed by
328 preplanned Tukey-HSD post-hoc comparisons across all groups. Local functional connectivity
329 maps were calculated for each voxel using threshold correlation (T_c) > 0.6, a signal-to-noise
330 ratio (T_{SNR} > 0.5), and distance < 1 mm in individual space and normalized to a z score with the
331 Fisher r to z transformation. Significance was assessed using same-sex Student's t-test
332 comparisons for different rearing conditions with Benjamini-Hochberg correction for multiple
333 comparisons with a false discovery rate (FDR) < 0.05 and local cluster size of k> 25 voxels.
334
335 **RESULTS**
336
337 ***LB Causes Sex-Specific Structural and Functional Synaptic Deficits in Adolescent Male***
338 ***Mice***
339 We have recently demonstrated that adolescent male LB mice exhibit more severe deficits in
340 contextual fear conditioning compared to female LB mice (Islam et al., 2023). Here, we
341 replicated these findings using an independent cohort of mice (Figure 1A-B). At the completion
342 of the behavioral testing, mice were processed to evaluate the effects of rearing and sex on
343 spine density and morphology using DiOlistic labeling (Figure 1C and Figure S1A). A 2 x 2
344 ANOVA revealed a significant effect of rearing on total spine density, with no significant main
345 effect of sex or interaction (Figure 1D). Sidak post-hoc analysis revealed a significant increase
346 in total spine density in males but not females (Figure 1D). The increase in spine density was
347 due to a higher number of immature spines, which was again significant in males but not
348 females (Figure 1E). A 2 x 2 ANOVA of the density of mature (mushroom) spines found
349 significant effects of rearing and sex, but no significant interaction. Sidak post-hoc analysis

350 indicated a significant decrease in the density of mushroom spines in males but not in females
351 (Figure 1F).
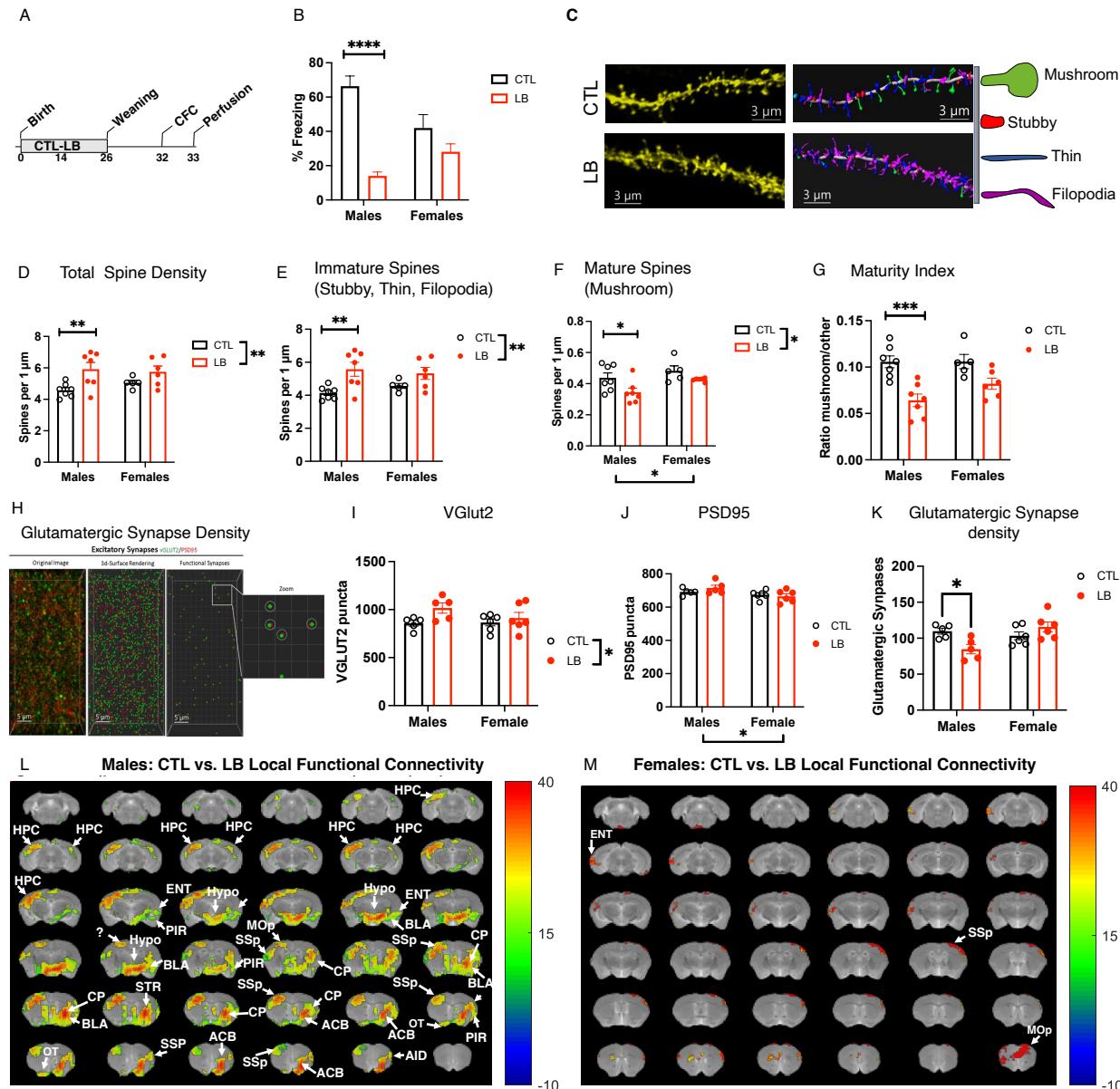
352
353 **Figure 1. LB Causes Sex-Specific Deficits in Contextual Freezing, Synaptic Maturity,**
354 **Synaptic Density and Local Functional Connectivity in LB Male Adolescent Mice**.
355 (A) Experimental Timeline.
356
357 (B) Contextual fear conditioning. Rearing: $F_{(1, 42)} = 34.44$, $P < 0.0001$, Sex: $F_{(1, 42)} = 0.84$, P=
358 0.36, Interaction: $F_{(1, 42)} = 11.63$ P=0.0014, CTL vs LB- males: P <0.0001, Cohen's d= 3.5,
359 females: P= 0.16, Cohen's d= 0.62. N= 11-15 mice per rearing and sex group.
360
361 (C) DiOlistic images and Imaris models of apical dendrites in the stratum radiatum in adolescent
362 CTL and LB mice. Mushroom spines (green), thin spines (blue), filopodia (magenta).
363

(D) Total Spine Density. Rearing: $F_{(1, 21)} = 10.19$, P=0.0044, $\eta_p^2 = 0.33$, Sex: $F_{(1, 21)} = 0.23$, P= 0.63, Interaction: $F_{(1, 21)} = 0.9$, P= 0.33. Sidak post-hoc analysis, CTL vs LB- males: P= 0.0093, Cohen's d= 1.57. CTL vs LB- females: P= 0.29, Cohen's d= 0.99.

(E) Density of Immature spines. Rearing: $F_{(1, 21)} = 11.99$, P= 0.0023, $\eta_p^2 = 0.36$, Sex $F_{(1, 21)} = 0.082$, P= 0.77, Interaction: $F_{(1, 21)} = 1.135$, P= 0.29. Sidak post-hoc analysis, CTL vs LB- males: P= 0.0051, Cohen's d= 1.71. CTL vs LB- females: P= 0.23, Cohen's d= 1.07.

(F) Mature spines. Rearing: $F_{(1, 21)} = 7.827$ P=0.011, $\eta_p^2 = 0.27$, Sex: $F_{(1, 21)} = 5.560$ P=0.0282, $\eta_p^2 = 0.21$, Interaction: $F_{(1, 21)} = 0.4883$, P= 0.49. Sidak post-hoc analysis, CTL vs LB- males: P= 0.03, Cohen's d= 1.22. CTL vs LB- females: P= 0.32, Cohen's d= 1.16.

(G) Maturity Index: Rearing: $F_{(1, 21)} = 23.28$, P< 0.0005, $\eta_p^2 = 0.53$, Sex: $F_{(1, 21)} = 1.789$, P=0.19, Interaction: $F_{(1, 21)} = 1.69$, P= 0.21. Sidak post-hoc analysis, CTL vs LB- males: P= 0.0003, Cohen's d= 2.38. CTL vs LB- females: P= 0.056, Cohen's d= 1.5.

(H) Confocal images and Imaris models used to calculate glutamatergic synapse density in the stratum radiatum.

(I) Density of VGlut2 puncta. Rearing: $F_{(1, 18)} = 4.816$, P= 0.041, $\eta_p^2 = 0.21$, Sex: $F_{(1, 18)} = 1.049$, P= 0.319, Interaction: $F_{(1, 18)} = 1.458$, P=0.24. Sidak post-hoc analysis, CTL vs LB- males: P= 0.067. CTL vs LB- females: P= 0.95.

(J) Density of PSD95 puncta. Rearing: $F_{(1, 18)} = 0.3042$, P= 0.58, Sex: $F_{(1, 18)} = 6.495$, P= 0.02, Interaction: $F_{(1, 18)} = 1.492$, P= 0.24.

(K) Density of glutamatergic synapses: Rearing: $F_{(1, 18)} = 1.119$, P= 0.30, Sex: $F_{(1, 18)} = 4.185$, P= 0.056, Interaction: $F_{(1, 18)} = 9.702$, P= 0.006, $\eta_p^2 = 0.35$. Sidak post-hoc analysis, CTL vs LB- males: P= 0.022, Cohen's d= 2.05. CTL vs LB- females: P= 0.29, Cohen's d= -0.81.

(L-M) Effects of rearing on local functional connectivity in males (L) and females (M), FDR < 0.05, local cluster size k> 25 voxels, N= 5-6 mice per rearing and sex group. Abbreviations: ACB- nucleus accumbens, AID- agranular insular area, BLA- basolateral amygdala, CP- caudoputamen, ENT- Entorhinal cortex, HPC- hippocampus, Hypo- hypothalamus, MOp- primary motor area, OT- olfactory tubercle, Pir- piriform area, SSp- primary sensory area.

We defined the "maturity index" as the ratio between mature mushroom spines and immature spines (e.g., filopodia, thin, stubby; Figure S1B) and found a significant effect of rearing, but no significant effect of sex or interaction (Figure 1G). Post-hoc analysis in males found a highly significant reduction in maturity index while only a trend was observed in LB females (Figure 1G). There was also a highly significant correlation between the maturity index and freezing behavior (r= 0.43, P= 0.007, Figure S1C).

Next, we evaluated the impact of rearing and sex on the density of glutamatergic synapses in the stratum radiatum (Figure 1H). For the presynaptic marker VGlut2, we found a significant effect of rearing, but no significant effects of sex or interaction. A preplanned Sidak post-hoc analysis revealed a non-significant trend for increased VGlut2 density in males and no difference in females (Figure 1I). For the excitatory postsynaptic marker PSD95, there was a significant effect of sex, with a small increase observed in males, but no significant effects of rearing or interaction (Figure 1J). Consistent with the DiOlistic results, we found a significant

414 interaction between LB and sex for the number of functional glutamatergic synapses. This was
415 due to a decrease in excitatory synapses in LB males but not in LB females (Figure 1K).
416
417 To investigate the impact of LB and sex on local functional connectivity throughout the entire
418 brain, we adopted an MRI-based method previously employed in human subjects (Tomasi and
419 Volkow, 2010) and applied it to rodents. This approach generates whole-brain voxel maps
420 corrected for multiple comparisons and unbiasedly identify brain regions with abnormal local
421 functional connectivity. Adolescent male LB mice showed reduced local connectivity in multiple
422 brain regions, including the hippocampus, entorhinal cortex, striatum, basolateral amygdala,
423 hypothalamus, and the nucleus accumbens (Figure 1L). In contrast, there was no reduction in
424 local functional connectivity in the hippocampus of LB females with only few brain regions
425 showing significantly lower local functional connectivity (Figure 1M). These findings reveal novel
426 sex differences in the impact of LB on contextual fear conditioning, maturity index, glutamatergic
427 synapse density, and local functional connectivity in the hippocampus of adolescent mice.
428
429 ***LB Transiently Impairs Microglial Function in the Developing Hippocampus***
430 LB impairs microglial ramification and their ability to engulf synaptic material at P17, an age
431 when the hippocampus undergoes intense synaptic pruning (Dayananda et al., 2022). To
432 determine if these changes persisted in P33 adolescent mice and whether they differentially
433 impacted males, we evaluated the effects of rearing, sex, and age in P17 and P33 mice. No
434 significant main effect or interaction with sex were found, so the data for males and females
435 were combined. A 2 x 2 ANOVA found a significant interaction between rearing and age for
436 microglial volume. Post-hoc analysis comparing CTL and LB P17 pups replicated our previous
437 work showing a significant reduction in microglial volume (Fig 2 A & B), CD68 volume (Fig 2 A &
438 C), the number of PSD96 engulfed by microglia (Fig 2 A & D), and the number of PSD95 inside
439 CD68 (Fig 2 A & D), all with large effect sizes. No significant differences between CTL and LB
440 survived multiple comparisons at P33 when using the entire set of data. A 2 x 2 ANOVA
441 examining the effects of rearing and sex at P33, revealed a significant increase in the number of
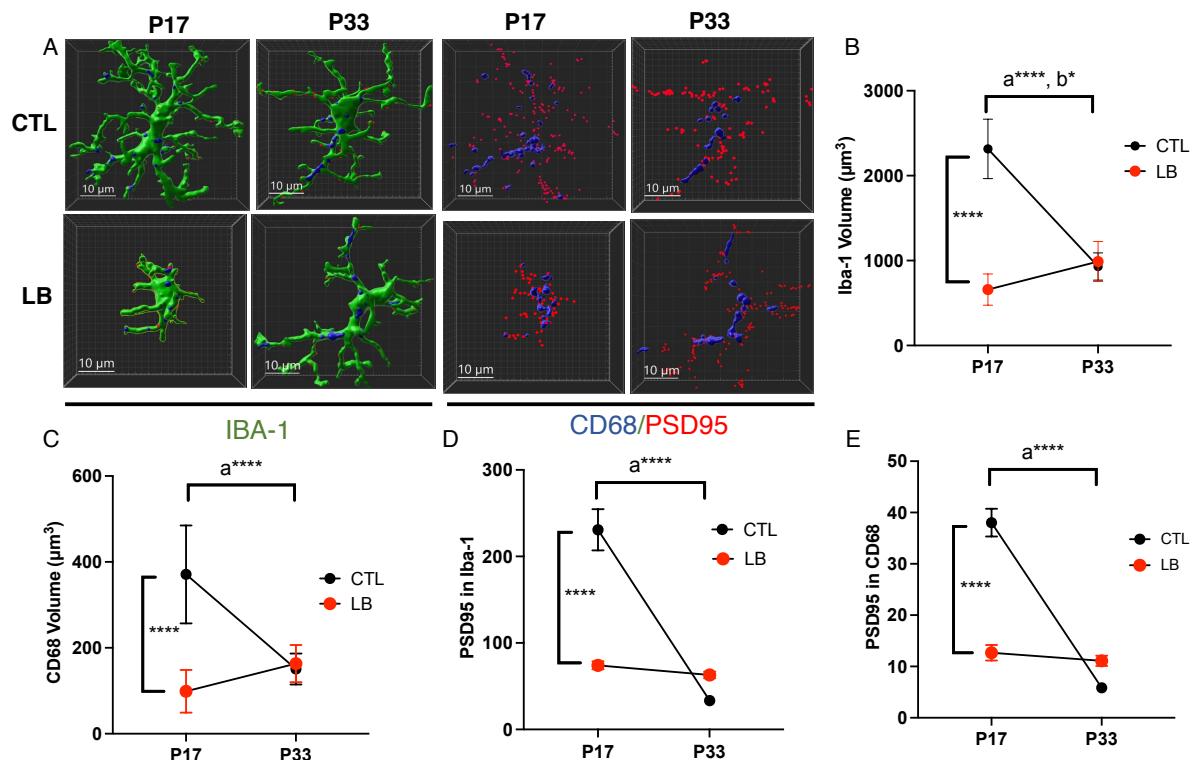
442   PSD95 puncta inside microglia (Fig S2C) and inside CD68 (Fig S2D) in LB male and female
443   mice, suggesting a possible compensatory microglial response at this age.
444
445   **Figure 2. LB Impairs Microglial Mediated Synaptic Pruning at P17 but not P33.**
446   (A) Imaris images of microglia (green, left panel) in CTL and LB P17 and P33 mice. CD68
447   phagosome staining (blue), and PSD95 puncta (red) of the same cells are shown in the right
448   panel. Scale bars 10um. N= 8 mice per rearing and age group, 50% females.
449
450   (B) Microglial volume. Rearing by age interaction: $F_{(1, 28)} = 98.95$ P<0.0001, $\eta_p^2 = 0.78$. CTL vs
451   LB P17: P< <0.0001, Cohen's d= 5.92. CTL vs LB P33: P= 0.63. P17 vs P33 CTL: P< 0.0001,
452   Cohen's d= 5.09 (shown as lower-case a). P17 vs P33 LB: P= 0.01, Cohen's d= -1.56 (shown as
453   lower-case b).
454
455   (C) CD68 volume. Rearing by age interaction: $F_{(1, 28)} = 34.82$ P<0.0001, $\eta_p^2 = 0.55$.
456   CTL vs LB P17: P< <0.0001 Cohen's d= 3.1. CTL vs LB P33: P= 0.35. P17 vs P33 CTL: P<
457   <0.0001 Cohen's d= 2.61 (lower-case a). P17 vs P33 LB: P= 0.25
458
459   (D), Number of PSD95 puncta inside microglia. Rearing by age interaction: $F_{(1, 28)} = 56.58$
460   P<0.0001, $\eta_p^2 = 0.67$. CTL vs LB P17: P< <0.000, Cohen's d= 3.23. CTL vs LB P3: P= 0.98. P17
461   vs P33 CTL P< <0.0001, Cohen's d= 4.1 (shown as a), P17 vs P33 LB: P= 0.92.
462
463   (E) Number of PSD95 puncta inside CD68 phagosome. Rearing by age interaction: $F_{(1, 28)} =$
464   86.90, P<0.0001, $\eta_p^2 = 0.75$. CTL vs LB P17: P< <0.0001, Cohen's d= 4.1. CTL vs LB P33: P=
465   0.18. P17 vs P33 CTL: P< <0.0001, Cohen's d= 5.88 (lower-case a). P17 vs P33 LB: P= 0.98.
466
467   CTL mice exhibited a dramatic reduction in microglial volume, phagosome size, and the number
468   of PSD95 engulfed by microglia at P33 compared to P17 (Figure 2). This is consistent with
469   previous work showing that synaptic pruning reaches its peak in the hippocampus during the
470   second and third weeks of life (Filipello et al., 2018; Scott-Hewitt et al., 2020; Zhan et al., 2014).
471   In contrast, LB microglia showed a small but significant increase in volume at P33 compared to
472   P17 (Figure 2B). However, there were no significant differences in CD68 size, PSD95 puncta
473   inside microglia, or PSD95 puncta inside CD68 between P17 and P33 (Figure 2 C-E). Together,
474   these findings indicate that LB impairs the ability of microglia to engulf synaptic material at P17.
475   These deficits are no longer observed at P33 when microglial phagocytic activity is significantly
476   lower.
477
478   ***Transient Ablation of Microglia Induces Sex-Specific Changes in the Hippocampus that***
479   ***Resemble Abnormalities Observed in LB Mice.***
480   Our data indicate that LB transiently impairs microglial phagocytic activity during the second and
481   third weeks of life when the hippocampus undergoes intense synaptic pruning. These changes
482   are associated with sex-specific impairments in contextual fear conditioning, maturity index,
483   glutamatergic synaptic densities, and local functional connectivity. To test whether transient
484   perturbation in microglial activity can induce similar sex-specific changes, we developed a
485   method to transiently ablate microglia during the 2nd-3rd weeks of life and tested the impact of
486   this manipulation on contextual fear conditioning, maturity index, glutamatergic synapse density,
487   and local functional connectivity in adolescent male and female mice. To transiently ablate
488   microglia, we mated CX3CR1-[Cre-ET2/ Cre-ET2]; ROSA26-eGFP-[DTA]/wt male mice with Balb/cByj
489   females to generate mixed litters that are either CX3CR1-[Cre-ET2/ WT]; ROSA26-eGFP-[DTA]/wt (DTA)
490   or CX3CR1-[Cre-ET2/ WT]; ROSA26-eGFP-[wt]/wt (WT) littermates (Fig 3A-B and Fig S2A).

491
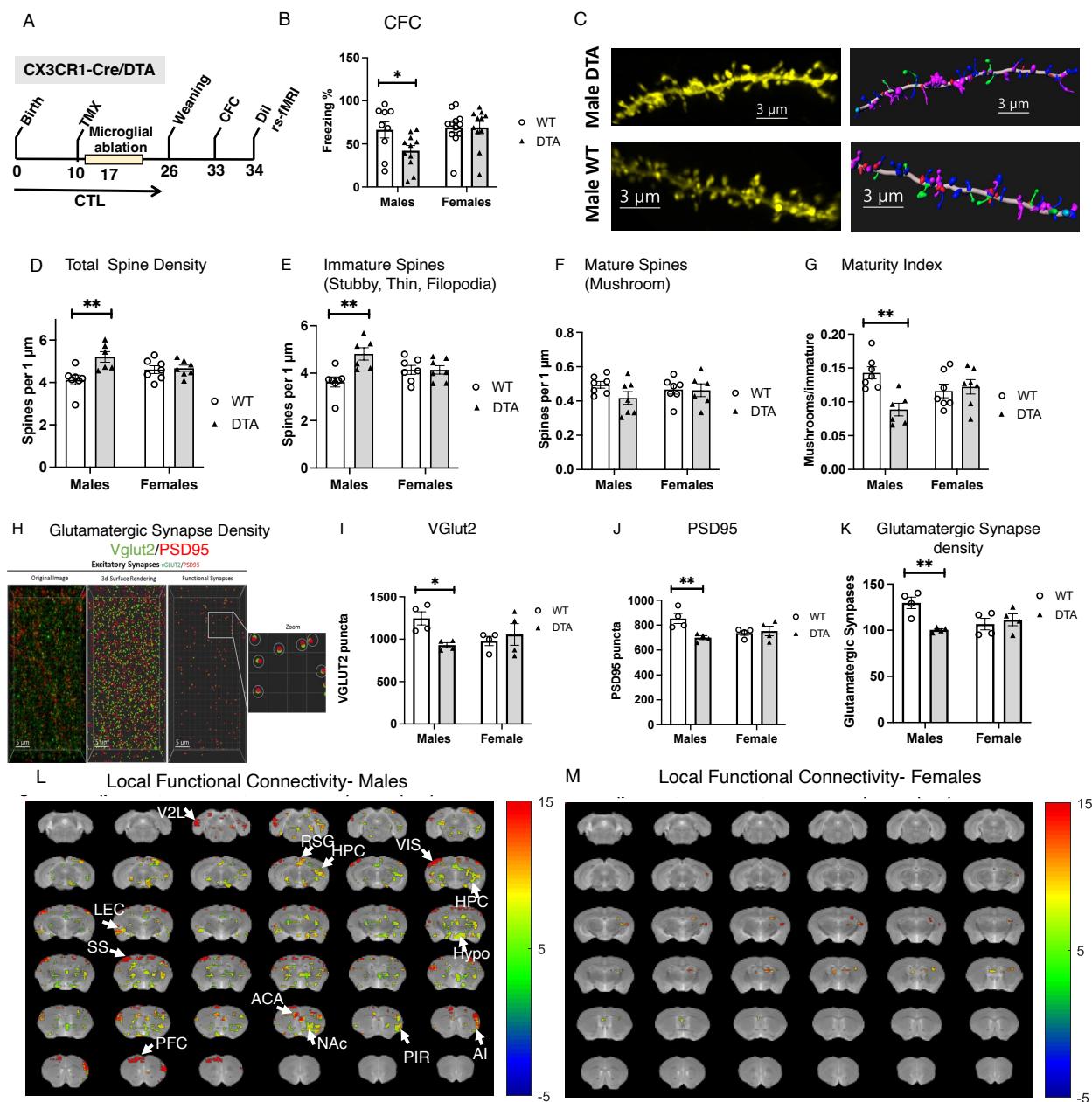
492

Figure 3. Transient Ablation of Microglia Induces Similar Sex-Specific Changes Observed in LB Adolescent Mice.

(A) Experimental Timeline.

B. Contextual fear conditioning. Genotype: $F_{(1, 39)}$ = 3.00, P=0.09, Sex: $F_{(1, 39)}$ = 4.49, P=0.04, Interaction: $F_{(1, 39)}$ = 2.98, P= 0.092. Post-hoc CTL vs LB- males: P= 0.046. CTL vs LB- females: P >0.99.

(C) Confocal images and Imaris models of DiOlistic labeling of apical dendrites in the stratum radiatum in adolescent WT and DTA male mice. Mushroom spines (green), thin spines (blue), filopodia (magenta).

(D) Total spine density. Genotype: $F_{(1, 23)}$ = 8.097, P= 0.0092, Sex: $F_{(1, 23)}$ = 0.012, P= 0.91, Interaction: $F_{(1, 23)}$ = 6.374, P=0.019. Post-hoc CTL vs LB- males: P= 0.0022. CTL vs LB- females: P= 0.97.

(E) Immature spines. Genotype: $F_{(1, 23)}$ = 8.020, P=0.0094, Sex: $F_{(1, 23)}$ = 0.1401, P=0.712, Interaction: $F_{(1, 23)}$ = 8.05, P= 0.0093. Post-hoc CTL vs LB- males: P= 0.0013. CTL vs LB- females: P >0.99.

(F). Mature Spines. Genotype: $F_{(1, 23)}$ = 1.788, P= 0.19, Sex: $F_{(1, 23)}$ = 0.078, P= 0.78, Interaction: $F_{(1, 23)}$ = 1.41, P= 0.25.

(G) Maturity Index. Genotype: $F_{(1, 23)}$ = 5.99, P= 0.022, Sex: $F_{(1, 23)}$ = 0.12, P= 0.731, Interaction: $F_{(1, 23)}$ = 9.425, P=0.0054. Post-hoc CTL vs LB- males: P= 0.0017. CTL vs LB- females: P= 0.88.

(H) Confocal images and Imaris models of VGlut2 and PSD95 puncta in the stratum radiatum.

(I) VGlut2 density. Genotype: $F_{(1, 12)}$ = 2.19, P= 0.16, Sex: $F_{(1, 12)}$ = 0.76, P= 0.39, Interaction: $F_{(1, 12)}$ = 5.874, P=0.032. Post-hoc CTL vs LB- males: P= 0.035. CTL vs LB- females: P> 0.99.

(J) PSD95 density. Genotype: $F_{(1, 12)}$ = 5.09, P= 0.043, Sex: $F_{(1, 12)}$ = 1.09, P= 0.32, Interaction: $F_{(1, 12)}$ = 7.827, P=0.016. Post-hoc CTL vs LB- males: P= 0.0077, Females: P> 0.99.

(K) Glutamatergic Synapse Density. Genotype: $F_{(1, 12)}$ = 5.014, P=0.04, Sex: $F_{(1, 12)}$ = 1.19, P= 0.29, Interaction: $F_{(1, 12)}$ = 9.58, P= 0.0093. Post-hoc CTL vs LB- males: P= 0.0053, females: P> 0.99.

(L-M) Local functional connectivity. Local functional connectivity maps of WT vs DTA males (L) and females (M), FDR < 0.05, local cluster size k> 25 voxels, N= 6 mice per rearing and sex group (red-yellow colors indicate reduced connectivity in DTA compared to WT mice). Abbreviations: ACA- Anterior Cingulate Area, AI- Anterior Insular area, V2L secondary visual lateral Cortex, RSG- retrosplenial granular area, HPC- hippocampus, VIS- visual cortex, LEC- lateral entorhinal cortex, Hypo- hypothalamus, NAc- nucleus accumbens, PIR- piriform area, SS- Somatosensory area, PFC- medial prefrontal cortex.

A single injection of tamoxifen at P10 induced rapid elimination of microglia in DTA, but not WT littermates with no signs of toxicity (Figure S3). By P21, the number and the morphology of microglia in the hippocampus of DTA mice were indistinguishable from WT littermates (Fig S3), consistent with previous work showing that a small pool of microglia survives the initial ablation and proliferates to restore normal number of microglia within 1-2 weeks (Bruttger et al., 2015; Nelson and Lenz, 2017; Rice et al., 2015; Schalbetter et al., 2022). Next, we tested the impact of transiently ablating microglia on contextual fear conditioning in adolescent mice raised under CTL condition (Fig 3A-B). Similar to findings with LB mice, transient ablation of microglia reduced contextual freezing in male DTA, but not female DTA mice (Figure 3B). DTA male mice, but not females showed an increase in the total number of spines (Figure 3 C-D) due to the retention of immature spines (Figure 3E). The mean number of mature mushroom spines was reduced in male DTA mice, but this did not reach significance (Figure 3F). The maturity index was reduced in DTA males, but not female adolescent mice (Figure 3G) and as with LB adolescent mice (Figure S1B), there was a significant correlation between the maturity index and freezing behavior (r= 0.74, P= 0.0027, Figure S1).

555
556 Unlike outcomes seen in adolescent LB mice, transient ablation of microglia decreased the
557 density of VGlut2 (Figure 3 H & I) and PSD95 (Figure 3 H & J) in males, but not females.
558 However, the density of functional glutamatergic synapses was reduced in DTA males but not in
559 female DTA (Figure 3 K), further highlighting similarities with LB mice (see Figure 1K). DTA
560 male mice had reduced local functional connectivity compared to WT littermates across multiple
561 brain regions, including the hippocampus (Figure 3L), changes that were not seen in DTA
562 females (Figure 3M). Together, these findings indicate that transient ablation of microglial during
563 the second and third weeks of life can replicate several of the sex-specific changes seen in the
564 hippocampus of LB adolescent mice.
565
566 ***Chemogenetic Activation of Microglia Restores Phagocytic Activity in P17 LB Mice.***
567 To test whether chemogenetic activation of microglia during the second and third weeks of life
568 can normalize microglial-mediated synaptic pruning in 17-day-old LB pups, we mated CX3CR1-
569 $^{Cre-ET2}/^{Cre-ET2}$; CAG-LSL-Gq-DREADD$^{Gq/WT}$ males to Balb/cByj females to generate mixed litters
570 that are either CX3CR1-$^{Cre-ET2}/^{WT}$; CAG-LSL-Gq-DREADD$^{Gq/WT}$ (abbreviated as Gq) or CX3CR1-
571 $^{Cre-ET2}/^{WT}$; CAG-LSL-Gq-DREADD$^{WT/WT}$ (abbreviated as WT) and randomized them to either CTL
572 or LB conditions. At P10 tamoxifen was administered to express the Gq-DREADD followed by
573 five daily injections of CNO from postnatal day 13 to 17. Pups were perfused 60 minutes after
574 the last CNO injection to assess microglial morphology and phagocytic activity (Figure 4 A-B).
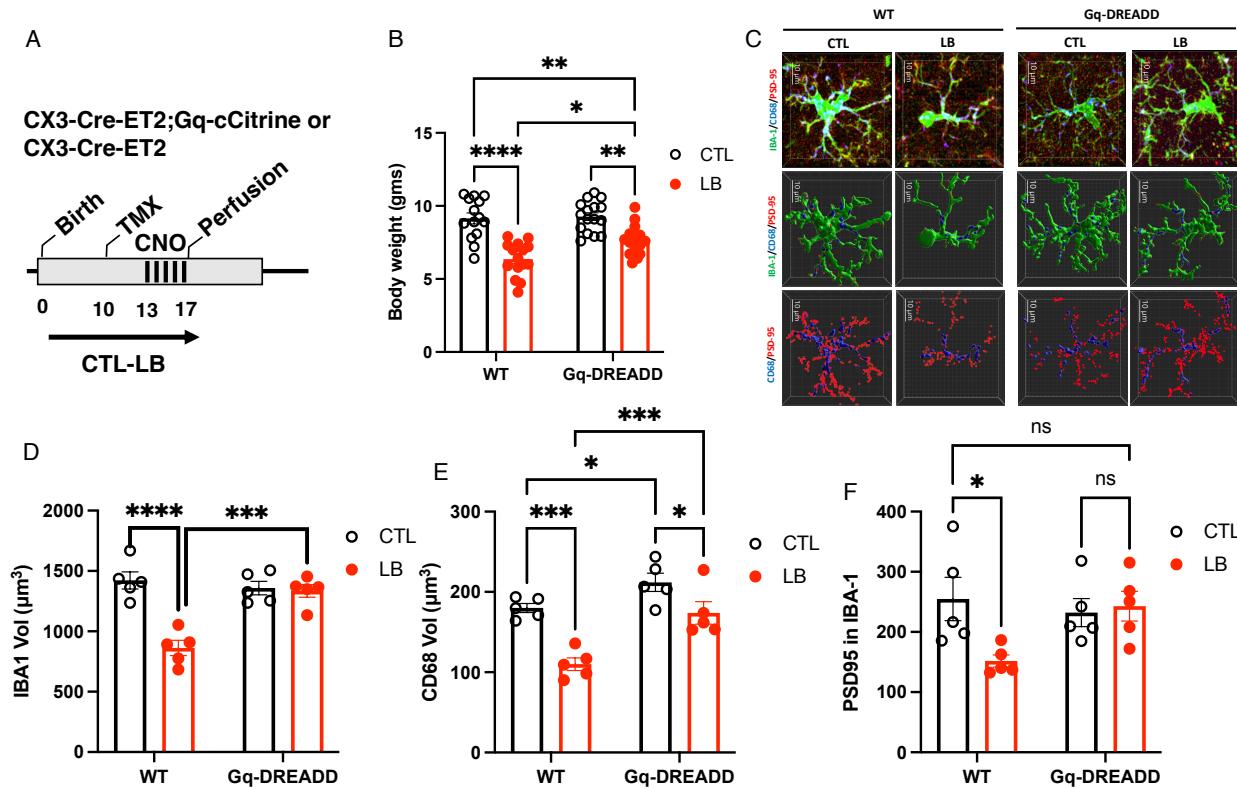
575
576 **Figure 4. *Chemogenetic Activation of Microglia Restores Normal Phagocytic Activity in***
577 ***P17 LB Mice***
578 (A) Experimental Timeline.
579
580 (B) Effects of rearing and genotype on body weight. Rearing: $F_{(1, 57)} = 55.87$, P< 0.0001,
581 Genotype: $F_{(1, 57)} = 5.714$, P= 0.020. Interaction: $F_{(1, 57)} = 3.86$, P= 0.054. Tukey-HSD post-

hoc CTL-WT vs LB-WT: P <0.0001. CTL-Gq vs LB-Gq: P= 0.0010, LB-WT vs LB-Gq: P= 0.015. CTL-WT vs LB-Gq: P= 0.0041. Half of the animals are females.

(C) Confocal and Imaris images of IBA1 (green), CD68 (blue), and PSD95 puncta (red) staining of microglia located in the stratum radiatum of P17 mice administered daily CNO injections from P13-17.

(D) Effects of rearing and genotype on microglial volume. Rearing: F (1, 16) = 22.88, P= 0.0002, Genotype: F (1, 16) = 11.25, P= 0.0040. Interaction: F (1, 16) = 19.35, P= 0.0004. Tukey-HSD post-hoc CTL-WT vs LB-WT: P <0.0001. CTL-Gq vs LB-Gq: P >0.99, LB-WT vs LB-Gq: P= 0.0003. CTL-WT vs LB-Gq: P >0.99. Half of the animals are females.

(E) Effects of rearing and genotype on CD68 volume. Rearing: F (1, 16) = 27.92, P< 0.0001, Genotype: F (1, 16) = 21.93, P= 0.0002. Interaction: F (1, 16) = 2.42, P= 0.14. Tukey-HSD post-hoc CTL-WT vs LB-WT: P= 0.0002. CTL-Gq vs LB-Gq: P= 0.0180, LB-WT vs LB-Gq: P= 0.0004. CTL-WT vs LB-Gq: P= 0.68. Half of the animals are females.

(F) Effects of rearing and genotype on PSD95 engulfed by microglia. Rearing: F (1, 16) = 3.35, P= 0.086, Genotype: F (1, 16) = 1.84, P=0.19. Interaction: F (1, 16) = 5.033, P= 0.039. Tukey-HSD post-hoc CTL-WT vs LB-WT: P= 0.048. CTL-Gq vs LB-Gq: P= 0.99, LB-WT vs LB-Gq: P= 0.09. CTL-WT vs LB-Gq: P= 0.99. Half of the animals are females.

All microglia from Gq mice expressed the HA tag, and no HA tag was expressed in microglia from WT mice (Figure S4). No sex differences or interaction with sex were found for any tested variables and therefore data from male and female mice were combined to determine main effects of rearing, genotype, and their interaction. For body weight, there was a significant main effect of rearing and genotype, with a trend for a significant interaction. Tukey-HSD post hoc analysis confirmed our previous work showing a reduction in body weight in LB pups. This was highly significant for CTL-WT vs LB-WT mice and to a lesser degree, although still significant, for CTL-Gq vs LB-Gq mice (Figure 4B). Interestingly, chemogenetic activation of microglia increased the body weight of LB (LB-WT vs LB-Gq) but not CTL mice (CTL-WT vs CTL-Gq) indicating that abnormal microglial activity contributes to the reduction in LB body weight. Chemogenetic activation increased the volume of microglia, CD68 size, and the number of PSD95 puncta inside microglia in LB-Gq pups to levels observed in CTL-WT pups with similar outcomes seen in males and females (Figure 4C-F). These findings indicate that chemogenetic activation of microglia during the second and third weeks of life normalizes microglia-mediated synaptic pruning in the developing hippocampus of mice exposed to LB.

Chemogenetic Activation of Microglia During the 2nd and 3rd Weeks of Life Restores Normal Hippocampal Function in Adolescent LB males.

Next, we tested whether chemogenetic activation of microglia from P13-17 can reverse the contextual fear conditioning deficits observed in adolescent LB mice (Figure 5A). A three-way ANOVA revealed a significant interaction between rearing, sex, and genotype (F (1, 107) = 5.643, P= 0.019), prompting us to conduct separate analyses in males and females. Males exhibited a significant interaction between rearing and genotype due to reduced freezing in LB-WT compared to CTL-WT and LB-Gq, with no significant differences between LB-Gq and LB-WT or CTL-WT mice (Figure 5B). As expected, no significant effects of rearing, genotype, and interaction were seen in females (Figure 5C). We then focused on the effects of chemogenetic activation on spine density and morphology in CA1 apical dendrites (Figure 5D). LB increased the total spine density in WT mice, but not in Gq mice, with no significant difference between CTL-WT and LB-Gq mice (Figure 5E), with similar outcomes observed for the number of

633   immature spines (Figure 5F). Chemogenetic activation also normalized the number of mature
634   spines in LB male mice (Figure 5G) and significantly increased the maturity index in LB-Gq mice
635   to levels observed in CTL-Gq mice, although it did not fully restore the maturity index to CTL-
636   WT levels (Figure 5F). The maturity index was again highly correlated with freezing behavior (r=
637   0.87, P= 0.001). LB increased the number of the presynaptic Vglut2 puncta in WT but not Gq
638   mice (Figure 5 I & J), while levels of PSD95 were unexpectedly higher in LB-Gq compared to
639   CTL-WT or CTL-Gq mice (Figure 5K). Chemogenetic activation completely restored the density
640   of functional glutamatergic synapses in the stratum radiatum (Figure 5L).
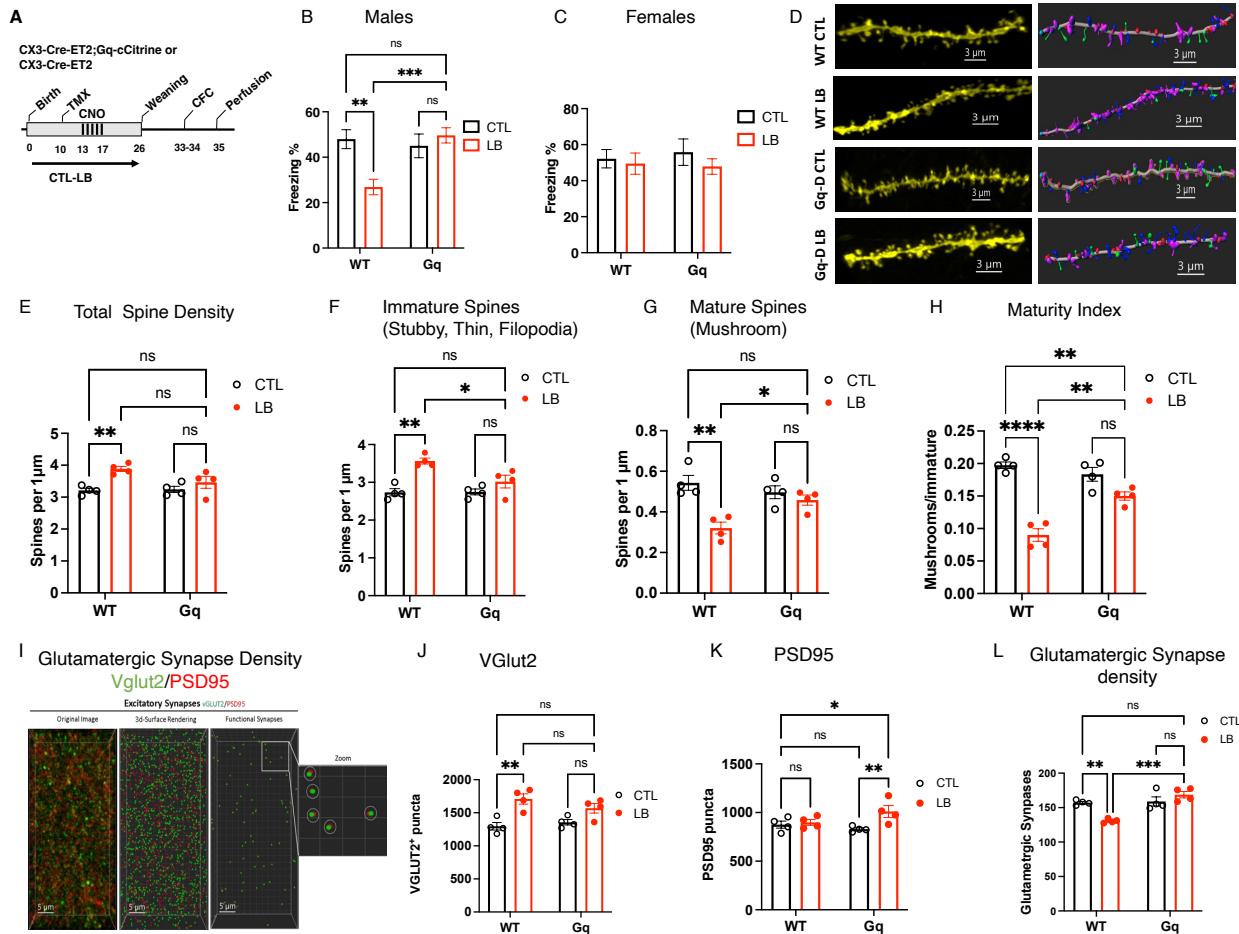
Fig 5. Chemogenetic Activation of Microglia During the Second and Third Weeks of Life Normalizes Contextual Fear Conditioning and Synaptic Abnormalities in Adolescent LB Males.

(A) Experimental timeline.

(B-C) contextual fear conditioning. (B) Males, n=12-19 mice per group. Rearing: F (1, 58) = 4.28, P= 0.043, Genotype F (1, 58) = 6.197, P=0.016, Interaction: F (1, 58) = 10.44, P=0.0020. CTL vs LB WT: P= 0.0011, CTL vs LB Gq: 0.97. LB-WT vs LB-Gq P= 0.0003, CTL-WT vs LB-Gq P= 0.99. (C) Females, n=11-18 mice per group. Rearing: F (1, 48) = 0.91, P= 0.35, Genotype: F (1, 48) = 0.033, P= 0.85, Interaction: F (1, 48) = 0.22, P= 0.64.

(D) Confocal images and Imaris models of DiOlistic labeling of apical dendrites in the stratum radiatum of adolescent male mice. Mushroom spines (green), thin spines (blue), filopodia (magenta).

(E) Total spine density. Rearing: $F_{(1, 12)} = 2.66$, P= 0.12, Genotype: $F_{(1, 12)} = 14.41$,P= 0.0025, Interaction: $F_{(1, 12)} = 3.66$, P= 0.07. CTL-WT vs LB-WT: P= 0.0077, CTL-Gq vs LB-Gq: P= 0.56. LB-WT vs LB-Gq P= 0.11, CTL-WT vs LB-Gq P= 0.45.

(F) Immature spines. Rearing: $F_{(1, 12)} = 5.74$, P= 0.0338, Genotype: $F_{(1, 12)} = 24.36$, P= 0.0003, Interaction: $F_{(1, 12)} = 6.172$, P=0.029. CTL-WT vs LB-WT: P= 0.0012, CTL-Gq vs LB-Gq: P= 0.49. LB-WT vs LB-Gq P= 0.028, CTL-WT vs LB-Gq P= 0.46.

(G) Mature spines. Rearing: $F_{(1, 12)} = 2.165$, P= 0.16, Genotype: $F_{(1, 12)} = 17.81$, P= 0.0012, Interaction: $F_{(1, 12)} = 8.84$, P= 0.0116. CTL-WT vs LB-WT: P= 0.0013, CTL-Gq vs LB-Gq: P= 0.81. LB-WT vs LB-Gq P= 0.037, CTL-WT vs LB-Gq P= 0.26.

(H) Maturity Index. Rearing: $F_{(1, 12)} = 7.79$, P= 0.016, Genotype: $F_{(1, 12)} = 72.83$, P< 0.0001, Interaction: $F_{(1, 12)} = 20.09$, P= 0.0008. CTL-WT vs LB-WT: P <0.0001, CTL-Gq vs LB-Gq: P= 0.082. LB-WT vs LB-Gq P= 0.0015, CTL-WT vs LB-Gq P= 0.0094.

(I) Confocal images and Imaris models of VGlut2 and PSD95 puncta in the stratum radiatum.

(J) VGlut2 density. Rearing: $F_{(1, 12)} = 24.22$, P= 0.0004, Genotype: $F_{(1, 12)} = 0.39$, P= 0.5437, Interaction: $F_{(1, 12)} = 2.47$, P= 0.14. CTL-WT vs LB-WT: P= 0.0037, CTL-Gq vs LB-Gq: P= 0.21. LB-WT vs LB-Gq: P= 0.87, CTL-WT vs LB-Gq: P= 0.062.

(K) PSD95 density. Rearing: $F_{(1, 12)} = 6.676$ P=0.024, Genotype: $F_{(1, 12)} = 0.68$, P= 0.42, Interaction: $F_{(1, 12)} = 4.068$, P=0.067. CTL-WT vs LB-WT: P= 0.69, CTL-Gq vs LB-Gq: P= 0.0069. LB-WT vs LB-Gq: P= 0.067, CTL-WT vs LB-Gq: P= 0.032.

(L) Glutamatergic synapse density. Rearing: $F_{(1, 12)} = 3.924$ P=0.071, Genotype: $F_{(1, 12)} = 22.36$, P= 0.0005, Interaction: $F_{(1, 12)} = 18.61$ P=0.0010. CTL-WT vs LB-WT: P= 0.0047, CTL-Gq vs LB-Gq: P= 0.75. LB-WT vs LB-Gq: P= 0.0002, CTL-WT vs LB-Gq: P= 0.45.

LB Increases MEGF10 and Phagocytic Activity in Females' Astrocytes

Our data suggest that during the second and third weeks of life, female LB mice are somehow able to compensate for deficits in microglial-mediated synaptic pruning. Given that astrocytes also play an important role in synaptic pruning and, in some cases, can compensate for abnormal microglia-mediated synaptic pruning (Chung et al., 2013; Damisah et al., 2020; Konishi et al., 2020; Lee et al., 2021; Perez-Catalan et al., 2021), we tested whether 17-day-old female LB mice can upregulate phagocytic activity in astrocytes (Figure S5A-B). No significant effects of rearing, sex, or their interaction were found for the number of GFAP-positive astrocytes in the stratum radiatum (Figure S5C). However, there was a significant interaction between rearing and sex for the number of PSD95 puncta per astrocyte and the density of PSD95 inside astrocytes. Post-hoc analysis revealed that this interaction was due to increase in PSD95 puncta in LB females but not in LB males (Figure S5 D-E). Previous studies have demonstrated that phagocytic activity in astrocytes is regulated by the MerTK and MEGF10 receptors (Chung et al., 2013; Lee et al., 2021). We therefore teste the levels of these receptors in LB male and female mice. No MerTK, staining was observed in GFAP-positive astrocytes in the stratum radiatum at this age. However, MEGF10 staining was clearly localized within GFAP-

705 positive cells (Figure 6). We therefore assessed the effects of rearing and sex on MEGF10 and
706 PSD95 puncta in astrocytes using a second cohort of 17-day-old pups (Figure 6A). There was a
707 significant effect of rearing, but no significant effects of sex or interaction for the volume of
708 GFAP-positive astrocytes located in the stratum radiatum (Figure 6B). We replicated our initial
709 findings, showing a significant increase in the number of PSD95 inside astrocytes in LB
710 females, but not LB males (Figure 6C and Fig S5). Additionally, this sex-specific effect was
711 accompanied by an increase in MEGF10 staining in astrocytes from LB females, but not LB
712 males (Figure 6D). Next, we investigated whether similar sex-specific changes were seen in 17-
713 day old mice exposed to transient ablation of microglia. Similar to outcomes seen in LB mice,
714 transient ablation of microglia led to an increase in the size of GFAP-positive astrocytes in
715 female subjects, but not in males (Fig S6A-B). However, unlike the outcomes in LB, microglial
716 ablation increased the number of PSD95 puncta and MEGF10 staining in both males and
717 females (Figure S6 C & D).
718
719
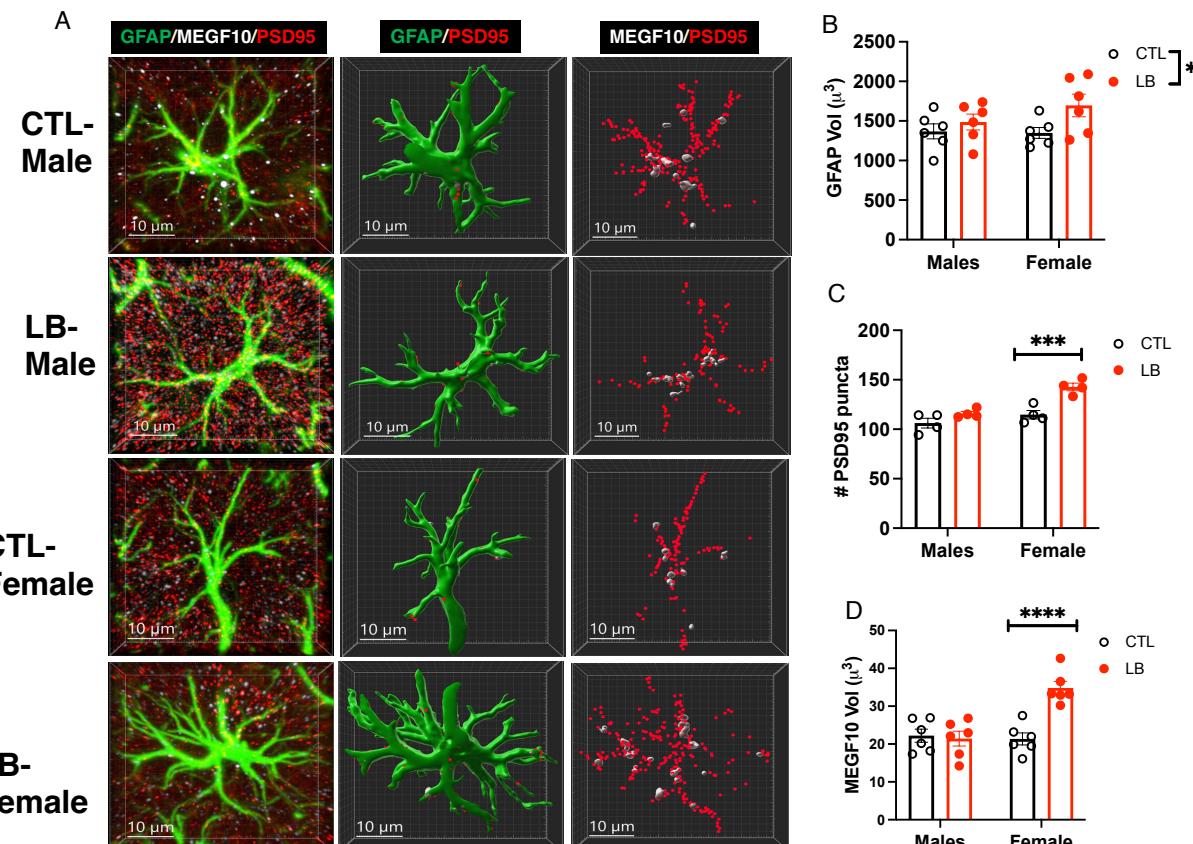
720
721
722 **Fig 6. LB Increases MEGF10 and Phagocytic Activity in Female Astrocytes**
723 (A) Confocal images and Imaris models of GFAP-positive astrocytes in the stratum radiatum of
724 17-day old CTL and LB pups. GFAP (green), PSD95 puncta (red), MEGF10 (white). Scale bar
725 10μm.
726
727 (B) Astrocyte cell volume. Rearing: $F_{(1, 20)} = 4.916$, P= 0.038, Sex: $F_{(1, 20)} = 0.82$, P= 0.38,
728 Interaction: $F_{(1, 20)} = 1.196$, P= 0.29. CTL vs LB Males: P= 0.68, CTL vs LB Females: P= 0.059.
729

730 (C) PSD95 puncta inside astrocyte. Rearing: $F_{(1, 12)} = 23.02$, P= 0.0004, Sex: $F_{(1, 12)} = 20.61$,
731 P= 0.0007, Interaction: $F_{(1, 12)} = 5.583$, P= 0.036, CTL vs LB Males: P= 0.2092, CTL vs LB
732 Females: P= 0.0006.

734 (D) MEGF10 staining inside astrocyte. Rearing: $F_{(1, 20)} = 12.92$, P= 0.0018, Sex: $F_{(1, 20)} =$
735 12.52, P= 0.0021, Interaction: $F_{(1, 20)} = 16.19$, P=0.0007, CTL vs LB Males: P= 0.76, CTL vs
736 LB Females: P< 0.0001.

738 **DISCUSSION**
739 One of the most consistent findings in individuals exposed to ELA is abnormal hippocampal
740 function, which seems to be more pronounced in men than in women (Garvin and Bolton, 2022;
741 Teicher and Samson, 2016; White and Kaffman, 2019). However, little is currently known about
742 the nature of these sex-specific structural and functional changes in the hippocampus and their
743 impact on cognition. Furthermore, it is unclear which forms of ELA cause sexually dimorphic
744 changes and what underlying mechanisms are responsible for the different outcomes in males
745 and females. These are difficult questions to address in humans, but they can be investigated in
746 rodent models of ELA and further validated with imaging techniques that can be used across
747 species (Kaffman et al., 2019). However, most of the research on rodents to date has focused
748 on changes in adult males. Therefore, additional studies are needed to examine changes in
749 both sexes, especially during adolescence when sex differences might be more prominent
750 (Gershon et al., 2008; White and Kaffman, 2019). Moreover, most studies have examined the
751 effects of ELA on neurons, with relatively little attention paid to the possible contribution of glial
752 cells. In particular, the role of microglia in inducing sexually dimorphic changes in ELA needs
753 further investigation, considering the crucial role of microglia in establishing sexually dimorphic
754 changes in the developing brain (VanRyzin et al., 2020) and sex-specific responses to pain,
755 obesity (Dorfman et al., 2017), and ischemia (Villa et al., 2018). This study presents several
756 novel findings about the role of glial cells in programming sexually dimorphic changes in the
757 hippocampus of adolescent mice exposed to LB, a commonly used mouse model of ELA.

759 ***LB causes sex-specific deficits in the stratum radiatum and contextual fear conditioning***
760 ***in adolescent mice.***
761 Our work supports the emerging notion that LB causes more severe hippocampal-dependent
762 deficits in males compared to females (Bath et al., 2017; Islam et al., 2023; Naninck et al.,
763 2015). Naninck and colleagues provided evidence indicating that these sex differences were
764 due to more severe deficits in adult neurogenesis in males (Naninck et al., 2015), but these
765 findings have not been replicated by others (Bath et al., 2017; Youssef et al., 2019). We have
766 recently shown that LB causes significant deficits in contextual fear conditioning in adolescent
767 male, but not female, mice (Islam et al., 2023). LB reduced hippocampal volume in both
768 adolescent male and female mice, indicating that LB female mice are also affected by LB and
769 that volumetric changes are unlikely to explain the sex-specific abnormalities in contextual fear
770 conditioning (Islam et al., 2023). Instead, we found that the connectivity between the entorhinal
771 cortex and the dorsal hippocampus was reduced fourfold in LB males but not in female mice.
772 Given the critical role that these projections play in mediating contextual fear conditioning we
773 proposed that changes in connectivity contribute to sex differences in hippocampal function
774 (Islam et al., 2023).

776 Here we examine the effects of rearing and sex on spine density and morphology of CA1
777 pyramidal neurons apical dendrites located in the stratum radiatum. These apical dendrites
778 receive input from CA3 pyramidal neurons via the Schaffer collaterals and play a critical role in
779 hippocampal mediated tasks such as contextual fear conditioning (Astudillo et al., 2020; Basu et
780 al., 2016; Li et al., 2005; Sacchetti et al., 2001; Sun et al., 2016). Using DiOlistic labeling we

781   found that LB male, but not LB female, mice show higher levels of immature spines (e.g.,
782   stubby, thin, filopodia) and low levels of mature mushroom spines. We found that the maturity
783   index is significantly reduced in male LB mice, but not females, and is highly correlated with
784   contextual freezing. Sex-specific deficits were also observed in the density of glutamatergic
785   synapse density in the stratum radiatum and local functional connectivity using rsfMRI.
786   Together, these findings uncover novel differences in synaptic function in the hippocampus of
787   adolescent male and female mice exposed to LB providing a likely explanation for the sex
788   differences seen in contextual fear conditioning. We provide evidence that alterations in glial
789   mediated synaptic pruning are likely to contribute to these sex-specific synaptic abnormalities,
790   but are mindful of the possibility that other processes, such as changes in connectivity between
791   the entorhinal cortex and the dorsal hippocampus, may also play a role.
792
793   ***LB Impairs Microglial Mediated Synaptic Pruning at P17 but not P33 Adolescent mice.***
794   Consistent with previous findings (Dayananda et al., 2022), we determined that LB causes
795   severe deficits in microglial mediated synaptic pruning during the second and third weeks of life,
796   and clarified that these abnormalities are no longer present in P33 adolescent LB mice.
797   Interestingly, the numbers of PSD95 puncta inside microglia or inside the phagosome were
798   roughly two-fold greater in adolescent (P33) LB compared to CTL mice. We hypothesize that
799   higher rates of synaptic pruning in adolescent LB mice may serve as a compensatory
800   mechanism to minimize the impact of deficits earlier in life but may also lead to "over pruning"
801   and cognitive deficits later in life. We show that the rate of synaptic engulfment is 7.6- fold
802   higher at P17 compared to P33 in CTL mice. This finding is consistent with previous work
803   showing that microglial mediated synaptic pruning peaks in the hippocampus during the second
804   and third weeks of life and that perturbation of this process leads to reduced connectivity in the
805   Schaffer collaterals later in life (Filipello et al., 2018; Scott-Hewitt et al., 2020; Zhan et al., 2014).
806   Zhan et al. (2014) have suggested that synaptic pruning is necessary for the formation of
807   multisynapse boutons 1(MSB1s). However, since MSB1s account for only 5% of all synaptic
808   boutons, a reduction in this small population of synaptic connections is unlikely to fully account
809   for the synaptic and cognitive deficits induced in response to abnormal microglial synaptic
810   pruning in the developing hippocampus. We propose that spine formation and maturation is a
811   competitive intracellular process for limited neuronal resources. The removal of non-functional
812   or weak spines during the second and third weeks of life is necessary to support the formation
813   of mature mushroom spines that are necessary for normal hippocampal function. The maturity
814   index provides a highly sensitive structural "footprint" for detecting earlier deficits in microglial-
815   mediated synaptic pruning. Importantly, both LB and transient ablation of microglia halve the
816   synaptic maturity index, and this index is strongly correlated with contextual fear conditioning.
817
818   ***Transient Elimination of Microglia Leads to Similar Sex-Specific Deficits Observed in LB***
819   ***Adolescent Mice***
820   This study is the first to investigate the effects of transiently ablating microglia during the second
821   and third weeks of life on hippocampal function in adolescent male and female mice. Our
822   findings indicate that microglia play a more prominent role in modulating synaptic plasticity and
823   contextual fear conditioning in male compared to female mice. These findings are supported by
824   research indicating that genomic differences between male and female microglia become
825   apparent during the second week of life (Hanamsagar et al., 2017; Thion et al., 2018).
826   Additionally, it has been shown that microglia have sex-specific impact on pain sensitivity
827   (Sorge et al., 2015), obesity (Dorfman et al., 2017), and neuroprotection against ischemic
828   strokes (Villa et al., 2018). Our findings are also consistent with studies showing that transient
829   perturbation of microglial function during a critical period of development results in long-term
830   alterations in synaptic plasticity and behavior (Bolton et al., 2022; Favuzzi et al., 2021; Garvin
831   and Bolton, 2022). For example, localized ablation of microglia in the prefrontal cortex of 6-

832   week-old male adolescent mice resulted in impaired working memory, decreased density of
833   mature mushroom spines, and reduced glutamatergic synapse density in adulthood. These
834   abnormalities were not observed when microglia were ablated in adult animals (Schalbetter et
835   al., 2022). Unfortunately, most ablation studies have been conducted exclusively in male mice.
836   However, the few studies that have examined both sexes found significant differences between
837   males and females (Bolton et al., 2022; Favuzzi et al., 2021; Garvin and Bolton, 2022). The
838   similarities between outcomes in adolescent LB mice and adolescent DTA mice (Figs 1 & 3)
839   support the idea that transient ablation of microglia contributes to sex differences in contextual
840   fear conditioning, maturity index, glutamatergic synapses, and local functional connectivity in the
841   hippocampus. The mechanisms responsible for the sex differences reported here in normally
842   developing DTA mice are yet to be elucidated, but it is possible that male mice have higher
843   rates of synapse formation compared to females. Assuming comparable rates of synapse
844   elimination in males and females (Figure 2 and Figure S6), elimination of microglia would thus
845   be expected to cause a more prominent reduction in the maturity index in males.
846
847   This is the first study to use rsfMRI to evaluate local functional connectivity in an animal model
848   of ELA. This approach provides an unbiased method to identify brain regions with presumed
849   differences in local connectivity (Tomasi and Volkow, 2010). However, to the best of our
850   knowledge, this is first example in which reduced local functional connectivity is linked to
851   reduced structural synaptic abnormalities. Using this approach, we identified several other brain
852   regions that show sex-specific changes in local connectivity in adolescent LB mice. These
853   include the entorhinal cortex, striatum, basolateral amygdala, nucleus accumbens, and the
854   hypothalamus. Additional work is required to further characterize the impact of LB and sex on
855   synaptic changes in these brain regions. It would be valuable to determine whether similar sex-
856   specific changes can be detected in humans exposed to various forms of ELA. Finally, the
857   observation that transient ablation of microglia reduces local functional connectivity in several
858   brain regions of normally developing adolescent mice suggests that this approach may provide
859   an indirect method to monitor microglial-mediated synaptic pruning during early development in
860   humans.
861
862   ***Chemogenetic Activation of Microglia During the Second and Third Weeks of Life***
863   ***Normalizes Microglial-Mediated Synaptic Pruning and Hippocampal Function***
864   Chemogenetic activation of microglia from P13-P17 was able to normalize microglial phagocytic
865   activity at P17 in LB male and female pups to levels seen in CTL. This, in turn, reversed the
866   deficits in contextual freezing and synaptic abnormalities observed in adolescent LB males.
867   These results align with recent findings indicating that chemogenetic activation of microglia
868   during the first week of life can restore normal glutamatergic innervation of CRH-positive cells in
869   the hypothalamus, adrenal size, and stress reactivity in male LB mice (Bolton et al., 2022). Our
870   findings demonstrate that increasing levels of microglial-mediated synaptic pruning during the
871   second and third weeks of life is sufficient to normalize the cognitive and synaptic abnormalities
872   observed in adolescent LB males and suggest that interventions enhancing microglial-mediated
873   synaptic pruning in childhood may offer an effective therapy for early adversities characterized
874   by low functional connectivity.
875
876   ***LB Increases MEGF10 and Astrocyte-Mediated Synaptic Pruning in the Developing***
877   ***Hippocampus of Female Mice.***
878   Previous work has shown that microglial mediated synaptic pruning in the hypothalamus is
879   impaired in 10-days old LB male, but not LB female, pups (Bolton et al., 2022). This was not the
880   case during peak synaptic pruning in the hippocampus where both male and female mice
881   showed pronounced deficits in microglial phagocytic activity in vivo and ex vivo (Dayananda et
882   al., 2022). Given that female adolescent mice show minimal synaptic and cognitive deficits and

883 that astrocytes can compensate for deficits in microglial-mediated synaptic pruning (Chung et
884 al., 2013; Damisah et al., 2020; Konishi et al., 2020; Lee et al., 2021; Perez-Catalan et al.,
885 2021), we assessed the effects of LB on synaptic pruning in astrocytes located in the stratum
886 radiatum. We found that LB increased the number of PSD95 puncta in astrocytes from female,
887 but not male, mice, an increase that was associated with upregulation of the MEGF10 receptor.
888 This is consistent with previous work showing that MEGF10 is necessary to support normal
889 synaptic pruning in astrocytes (Chung et al., 2013; Lee et al., 2021) and suggest a mechanism
890 by which female LB mice are able to compensate for microglial-mediated synaptic deficits.
891 Future studies will test whether cell-specific deletion of MEGF10 in astrocytes render females
892 more sensitive to LB-mediated changes in hippocampal function. Furthermore, clarifying the
893 mechanisms by which females upregulate the MEGF10 receptor, may offer novel strategies for
894 minimizing hippocampal-dependent synaptic and cognitive deficits in male LB mice.
895
896 ***Conclusions***
897 A better understanding of the underlying pathophysiology through which ELA alters
898 hippocampal function in both males and females is essential for the development of more
899 effective therapies. Here we show that LB causes more severe deficits in contextual freezing
900 and synaptic plasticity in adolescent male compared to female mice. At P17, when synaptic
901 pruning peaks in the hippocampus, both male and female pups exhibit a fourfold reduction in
902 microglial-mediated synaptic pruning. This is no longer the case at P33 when the rate of
903 microglial-mediated synaptic pruning is significantly lower. Transient ablation of microglia during
904 the second and third weeks of life leads to sex-specific deficits similar to those observed in LB
905 adolescent mice. Chemogenetic activation of microglia during the same period is sufficient to
906 reverse the contextual and synaptic abnormalities observed in LB male adolescent mice.
907 Finally, levels of MEGF10 and synaptic engulfment are elevated in 17-day-old LB females,
908 suggesting a potential compensatory mechanism for reducing the microglial-mediated
909 abnormalities in LB females. These studies highlight a novel role for glial cells in mediating sex-
910 specific hippocampal deficits in a mouse model of ELA.
911
912 **AKNOWLEDGMENTS**
915
916
917 **CONFLICT OF INTEREST**
918 The authors declare no conflict of interest.
919
920
921
922
923
924
925
926
927
928
929
930
931
932
933

REFERENCES

Anda, R.F., Felitti, V.J., Bremner, J.D., Walker, J.D., Whitfield, C., Perry, B.D., Dube, S.R., Giles, W.H., 2006. The enduring effects of abuse and related adverse experiences in childhood. A convergence of evidence from neurobiology and epidemiology. Eur Arch Psychiatry Clin Neurosci 256, 174-186.

Astudillo, D., Karmelic, D., Casas, B.S., Otmakhov, N., Palma, V., Sanhueza, M., 2020. CaMKII inhibitor 1 (CaMK2N1) mRNA is upregulated following LTP induction in hippocampal slices. Synapse 74, e22158.

Basu, J., Zaremba, J.D., Cheung, S.K., Hitti, F.L., Zemelman, B.V., Losonczy, A., Siegelbaum, S.A., 2016. Gating of hippocampal activity, plasticity, and memory by entorhinal cortex long-range inhibition. Science 351, aaa5694.

Bath, K.G., Nitenson, A.S., Lichtman, E., Lopez, C., Chen, W., Gallo, M., Goodwill, H., Manzano-Nieves, G., 2017. Early life stress leads to developmental and sex selective effects on performance in a novel object placement task. Neurobiology of stress 7, 57-67.

Bolton, J.L., Short, A.K., Othy, S., Kooiker, C.L., Shao, M., Gunn, B.G., Beck, J., Bai, X., Law, S.M., Savage, J.C., Lambert, J.J., Belelli, D., Tremblay, M.E., Cahalan, M.D., Baram, T.Z., 2022. Early stress-induced impaired microglial pruning of excitatory synapses on immature CRH-expressing neurons provokes aberrant adult stress responses. Cell reports 38, 110600.

Bruttger, J., Karram, K., Wortge, S., Regen, T., Marini, F., Hoppmann, N., Klein, M., Blank, T., Yona, S., Wolf, Y., Mack, M., Pinteaux, E., Muller, W., Zipp, F., Binder, H., Bopp, T., Prinz, M., Jung, S., Waisman, A., 2015. Genetic Cell Ablation Reveals Clusters of Local Self-Renewing Microglia in the Mammalian Central Nervous System. Immunity 43, 92-106.

Chung, W.S., Clarke, L.E., Wang, G.X., Stafford, B.K., Sher, A., Chakraborty, C., Joung, J., Foo, L.C., Thompson, A., Chen, C., Smith, S.J., Barres, B.A., 2013. Astrocytes mediate synapse elimination through MEGF10 and MERTK pathways. Nature 504, 394-400.

Crozier, J.C., Wang, L., Huettel, S.A., De Bellis, M.D., 2014. Neural correlates of cognitive and affective processing in maltreated youth with posttraumatic stress symptoms: does gender matter? Dev Psychopathol 26, 491-513.

Damisah, E.C., Hill, R.A., Rai, A., Chen, F., Rothlin, C.V., Ghosh, S., Grutzendler, J., 2020. Astrocytes and microglia play orchestrated roles and respect phagocytic territories during neuronal corpse removal in vivo. Sci Adv 6, eaba3239.

Dayananda, K.K., Ahmed, S., Wang, D., Polis, B., Islam, R., Kaffman, A., 2022. Early life stress impairs synaptic pruning in the developing hippocampus. Brain, behavior, and immunity.

De Bellis, M.D., Woolley, D.P., Hooper, S.R., 2013. Neuropsychological findings in pediatric maltreatment: relationship of PTSD, dissociative symptoms, and abuse/neglect indices to neurocognitive outcomes. Child Maltreat 18, 171-183.

Dorfman, M.D., Krull, J.E., Douglass, J.D., Fasnacht, R., Lara-Lince, F., Meek, T.H., Shi, X., Damian, V., Nguyen, H.T., Matsen, M.E., Morton, G.J., Thaler, J.P., 2017. Sex differences in

973   microglial CX3CR1 signalling determine obesity susceptibility in mice. Nature communications
974   8, 14556.

975   Farina, M.G., Sandhu, M.R.S., Parent, M., Sanganahalli, B.G., Derbin, M., Dhaher, R., Wang,
976   H., Zaveri, H.P., Zhou, Y., Danbolt, N.C., Hyder, F., Eid, T., 2021. Small loci of astroglial
977   glutamine synthetase deficiency in the postnatal brain cause epileptic seizures and impaired
978   functional connectivity. Epilepsia 62, 2858-2870.

979   Favuzzi, E., Huang, S., Saldi, G.A., Binan, L., Ibrahim, L.A., Fernandez-Otero, M., Cao, Y.,
980   Zeine, A., Sefah, A., Zheng, K., Xu, Q., Khlestova, E., Farhi, S.L., Bonneau, R., Datta, S.R.,
981   Stevens, B., Fishell, G., 2021. GABA-receptive microglia selectively sculpt developing inhibitory
982   circuits. Cell 184, 4048-4063 e4032.

983   Filipello, F., Morini, R., Corradini, I., Zerbi, V., Canzi, A., Michalski, B., Erreni, M., Markicevic,
984   M., Starvaggi-Cucuzza, C., Otero, K., Piccio, L., Cignarella, F., Perrucci, F., Tamborini, M.,
985   Genua, M., Rajendran, L., Menna, E., Vetrano, S., Fahnestock, M., Paolicelli, R.C., Matteoli, M.,
986   2018. The Microglial Innate Immune Receptor TREM2 Is Required for Synapse Elimination and
987   Normal Brain Connectivity. Immunity 48, 979-991 e978.

988   Forlano, P.M., Woolley, C.S., 2010. Quantitative analysis of pre- and postsynaptic sex
989   differences in the nucleus accumbens. J Comp Neurol 518, 1330-1348.

990   Garvin, M.M., Bolton, J.L., 2022. Sex-specific behavioral outcomes of early-life adversity and
991   emerging microglia-dependent mechanisms. Frontiers in behavioral neuroscience 16, 1013865.

992   Gershon, A., Minor, K., Hayward, C., 2008. Gender, victimization, and psychiatric outcomes.
993   Psychol Med 38, 1377-1391.

994   Green, J.G., McLaughlin, K.A., Berglund, P.A., Gruber, M.J., Sampson, N.A., Zaslavsky, A.M.,
995   Kessler, R.C., 2010. Childhood adversities and adult psychiatric disorders in the national
996   comorbidity survey replication I: associations with first onset of DSM-IV disorders. Arch Gen
997   Psychiatry 67, 113-123.

998   Hanamsagar, R., Alter, M.D., Block, C.S., Sullivan, H., Bolton, J.L., Bilbo, S.D., 2017.
999   Generation of a microglial developmental index in mice and in humans reveals a sex difference
1000   in maturation and immune reactivity. Glia 65, 1504-1520.

1001   Islam, R., White, D.R., Arefin, T.M., Mehta, S., Liu, X., Polis, B., Giuliano, L., Ahmed, S.,
1002   Bowers, C., Zhang, J., Kaffman, A., 2023. Early Deprivation Impairs Perforant Pathway
1003   Connectivity and Contextual Memory in Adolescent Male Mice. BioRxiv.

1004   Johnson, F.K., Delpech, J.C., Thompson, G.J., Wei, L., Hao, J., Herman, P., Hyder, F.,
1005   Kaffman, A., 2018. Amygdala hyper-connectivity in a mouse model of unpredictable early life
1006   stress. Translational psychiatry 8, 49.

1007   Johnson, F.K., Kaffman, A., 2017. Early life stress perturbs the function of microglia in the
1008   developing rodent brain: new insights and future challenges. Brain, behavior, and immunity.

1009   Kaffman, A., Meaney, M.J., 2007. Neurodevelopmental sequelae of postnatal maternal care in
1010   rodents: clinical and research implications of molecular insights. J Child Psychol Psychiatry 48,
1011   224-244.

Kaffman, A., White, J.D., Wei, L., Johnson, F.K., Krystal, J.H., 2019. Enhancing the Utility of Preclinical Research in Neuropsychiatry Drug Development. Methods Mol Biol 2011, 3-22.

Konishi, H., Okamoto, T., Hara, Y., Komine, O., Tamada, H., Maeda, M., Osako, F., Kobayashi, M., Nishiyama, A., Kataoka, Y., Takai, T., Udagawa, N., Jung, S., Ozato, K., Tamura, T., Tsuda, M., Yamanaka, K., Ogi, T., Sato, K., Kiyama, H., 2020. Astrocytic phagocytosis is a compensatory mechanism for microglial dysfunction. EMBO J 39, e104464.

Lambert, H.K., Peverill, M., Sambrook, K.A., Rosen, M.L., Sheridan, M.A., McLaughlin, K.A., 2019. Altered development of hippocampus-dependent associative learning following early-life adversity. Developmental cognitive neuroscience 38, 100666.

Lee, J.H., Kim, J.Y., Noh, S., Lee, H., Lee, S.Y., Mun, J.Y., Park, H., Chung, W.S., 2021. Astrocytes phagocytose adult hippocampal synapses for circuit homeostasis. Nature 590, 612-617.

Li, Z., Zhou, Q., Li, L., Mao, R., Wang, M., Peng, W., Dong, Z., Xu, L., Cao, J., 2005. Effects of unconditioned and conditioned aversive stimuli in an intense fear conditioning paradigm on synaptic plasticity in the hippocampal CA1 area in vivo. Hippocampus 15, 815-824.

McLaughlin, K.A., Colich, N.L., Rodman, A.M., Weissman, D.G., 2020. Mechanisms linking childhood trauma exposure and psychopathology: a transdiagnostic model of risk and resilience. BMC medicine 18, 96.

Naninck, E.F., Hoeijmakers, L., Kakava-Georgiadou, N., Meesters, A., Lazic, S.E., Lucassen, P.J., Korosi, A., 2015. Chronic early life stress alters developmental and adult neurogenesis and impairs cognitive function in mice. Hippocampus 25, 309-328.

Nelson, L.H., Lenz, K.M., 2017. Microglia depletion in early life programs persistent changes in social, mood-related, and locomotor behavior in male and female rats. Behav Brain Res 316, 279-293.

Nemeroff, C.B., 2016. Paradise Lost: The Neurobiological and Clinical Consequences of Child Abuse and Neglect. Neuron 89, 892-909.

Perez-Catalan, N.A., Doe, C.Q., Ackerman, S.D., 2021. The role of astrocyte-mediated plasticity in neural circuit development and function. Neural Dev 16, 1.

Rice, R.A., Spangenberg, E.E., Yamate-Morgan, H., Lee, R.J., Arora, R.P., Hernandez, M.X., Tenner, A.J., West, B.L., Green, K.N., 2015. Elimination of Microglia Improves Functional Outcomes Following Extensive Neuronal Loss in the Hippocampus. J Neurosci 35, 9977-9989.

Rocha, M., Wang, D., Avila-Quintero, V., Bloch, M.H., Kaffman, A., 2021. Deficits in hippocampal-dependent memory across different rodent models of early life stress: systematic review and meta-analysis. Translational psychiatry 11, 231.

Sacchetti, B., Lorenzini, C.A., Baldi, E., Bucherelli, C., Roberto, M., Tassoni, G., Brunelli, M., 2001. Long-lasting hippocampal potentiation and contextual memory consolidation. Eur J Neurosci 13, 2291-2298.

1049 Sanganahalli, B.G., Chitturi, J., Herman, P., Elkabes, S., Heary, R., Hyder, F., Kannurpatti, S.S.,
1050 2021. Supraspinal Sensorimotor and Pain-Related Reorganization after a Hemicontusion Rat
1051 Cervical Spinal Cord Injury. J Neurotrauma 38, 3393-3405.

1052 Schalbetter, S.M., von Arx, A.S., Cruz-Ochoa, N., Dawson, K., Ivanov, A., Mueller, F.S., Lin,
1053 H.Y., Amport, R., Mildenberger, W., Mattei, D., Beule, D., Foldy, C., Greter, M., Notter, T.,
1054 Meyer, U., 2022. Adolescence is a sensitive period for prefrontal microglia to act on cognitive
1055 development. Sci Adv 8, eabi6672.

1056 Scott-Hewitt, N., Perrucci, F., Morini, R., Erreni, M., Mahoney, M., Witkowska, A., Carey, A.,
1057 Faggiani, E., Schuetz, L.T., Mason, S., Tamborini, M., Bizzotto, M., Passoni, L., Filipello, F.,
1058 Jahn, R., Stevens, B., Matteoli, M., 2020. Local externalization of phosphatidylserine mediates
1059 developmental synaptic pruning by microglia. EMBO J 39, e105380.

1060 Sorge, R.E., Mapplebeck, J.C., Rosen, S., Beggs, S., Taves, S., Alexander, J.K., Martin, L.J.,
1061 Austin, J.S., Sotocinal, S.G., Chen, D., Yang, M., Shi, X.Q., Huang, H., Pillon, N.J., Bilan, P.J.,
1062 Tu, Y., Klip, A., Ji, R.R., Zhang, J., Salter, M.W., Mogil, J.S., 2015. Different immune cells
1063 mediate mechanical pain hypersensitivity in male and female mice. Nat Neurosci 18, 1081-
1064 1083.

1065 Sun, Y.Y., Cai, W., Yu, J., Liu, S.S., Zhuo, M., Li, B.M., Zhang, X.H., 2016. Surface expression
1066 of hippocampal NMDA GluN2B receptors regulated by fear conditioning determines its
1067 contribution to memory consolidation in adult rats. Scientific reports 6, 30743.

1068 Teicher, M.H., Samson, J.A., 2016. Annual Research Review: Enduring neurobiological effects
1069 of childhood abuse and neglect. J Child Psychol Psychiatry 57, 241-266.

1070 Thion, M.S., Low, D., Silvin, A., Chen, J., Grisel, P., Schulte-Schrepping, J., Blecher, R., Ulas,
1071 T., Squarzoni, P., Hoeffel, G., Coulpier, F., Siopi, E., David, F.S., Scholz, C., Shihui, F., Lum, J.,
1072 Amoyo, A.A., Larbi, A., Poidinger, M., Buttgereit, A., Lledo, P.M., Greter, M., Chan, J.K.Y., Amit,
1073 I., Beyer, M., Schultze, J.L., Schlitzer, A., Pettersson, S., Ginhoux, F., Garel, S., 2018.
1074 Microbiome Influences Prenatal and Adult Microglia in a Sex-Specific Manner. Cell 172, 500-
1075 516 e516.

1076 Tomasi, D., Volkow, N.D., 2010. Ultrafast method for mapping local functional connectivity hubs
1077 in the human brain. Annu Int Conf IEEE Eng Med Biol Soc 2010, 4274-4277.

1078 VanRyzin, J.W., Marquardt, A.E., Pickett, L.A., McCarthy, M.M., 2020. Microglia and sexual
1079 differentiation of the developing brain: A focus on extrinsic factors. Glia 68, 1100-1113.

1080 Villa, A., Gelosa, P., Castiglioni, L., Cimino, M., Rizzi, N., Pepe, G., Lolli, F., Marcello, E., Sironi,
1081 L., Vegeto, E., Maggi, A., 2018. Sex-Specific Features of Microglia from Adult Mice. Cell reports
1082 23, 3501-3511.

1083 White, J.D., Arefin, T.M., Pugliese, A., Lee, C.H., Gassen, J., Zhang, J., Kaffman, A., 2020.
1084 Early life stress causes sex-specific changes in adult fronto-limbic connectivity that differentially
1085 drive learning. Elife 9.

1086 White, J.D., Kaffman, A., 2019. The Moderating Effects of Sex on Consequences of Childhood
1087 Maltreatment: From Clinical Studies to Animal Models. Frontiers in neuroscience 13, 1082.

1088   Yanguas-Casás, N., 2020. Physiological sex differences in microglia and their
1089   relevance in neurological disorders. Neuroimmunol Neuroinflamation 7, 13-22.

1090   Youssef, M., Atsak, P., Cardenas, J., Kosmidis, S., Leonardo, E.D., Dranovsky, A., 2019. Early
1091   life stress delays hippocampal development and diminishes the adult stem cell pool in mice.
1092   Scientific reports 9, 4120.

1093   Zhan, Y., Paolicelli, R.C., Sforazzini, F., Weinhard, L., Bolasco, G., Pagani, F., Vyssotski, A.L.,
1094   Bifone, A., Gozzi, A., Ragozzino, D., Gross, C.T., 2014. Deficient neuron-microglia signaling
1095   results in impaired functional brain connectivity and social behavior. Nat Neurosci 17, 400-406.
1096

Supplemental Information. Ahmed et al. 2024
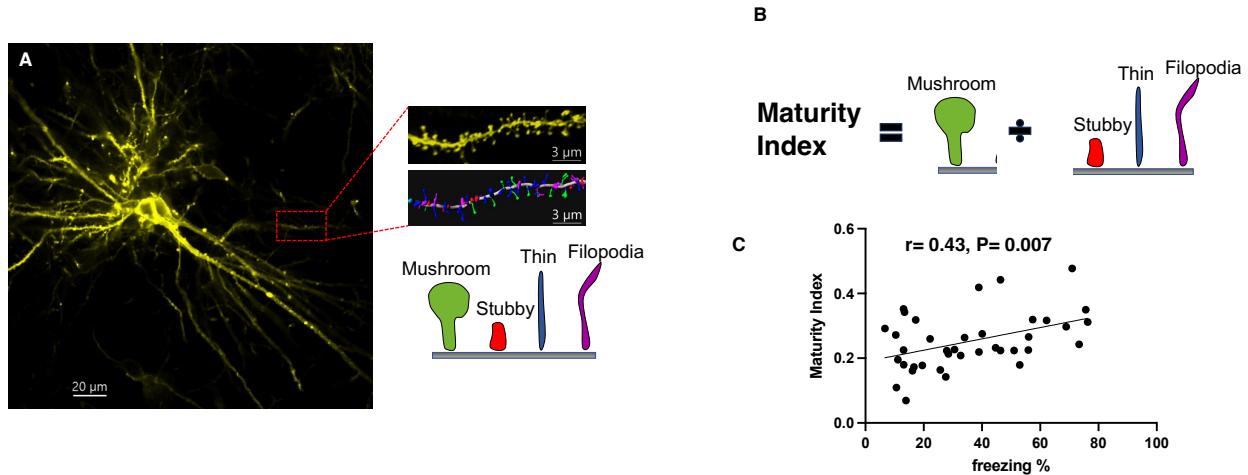
Fig S1. The Maturity Index Correlates with Contextual Fear Conditioning. (A) A representative low magnification image of CA1 pyramidal neuron labeled with DiI (Left). High magnification of a secondary apical dendrite and an Imaris color-coded model of spine morphology. (B) The ratio between the number of mushroom spines and all other spines was calculated for each apical dendrite and then averaged across 5-6 dendrites to quantify the maturity index for each mouse. (C) The maturity index is correlated with contextual fear conditioning in adolescent CTL and LB mice. Significant correlation between the maturity index and contextual fear conditioning was also seen in WT and DTA adolescent mice (r= 0.74, P= 0.0027, n= 14), and in adolescent mice in which microglia were chemogenetically activated from P13-17 (r= 0.87, P= 0.001, n= 16).
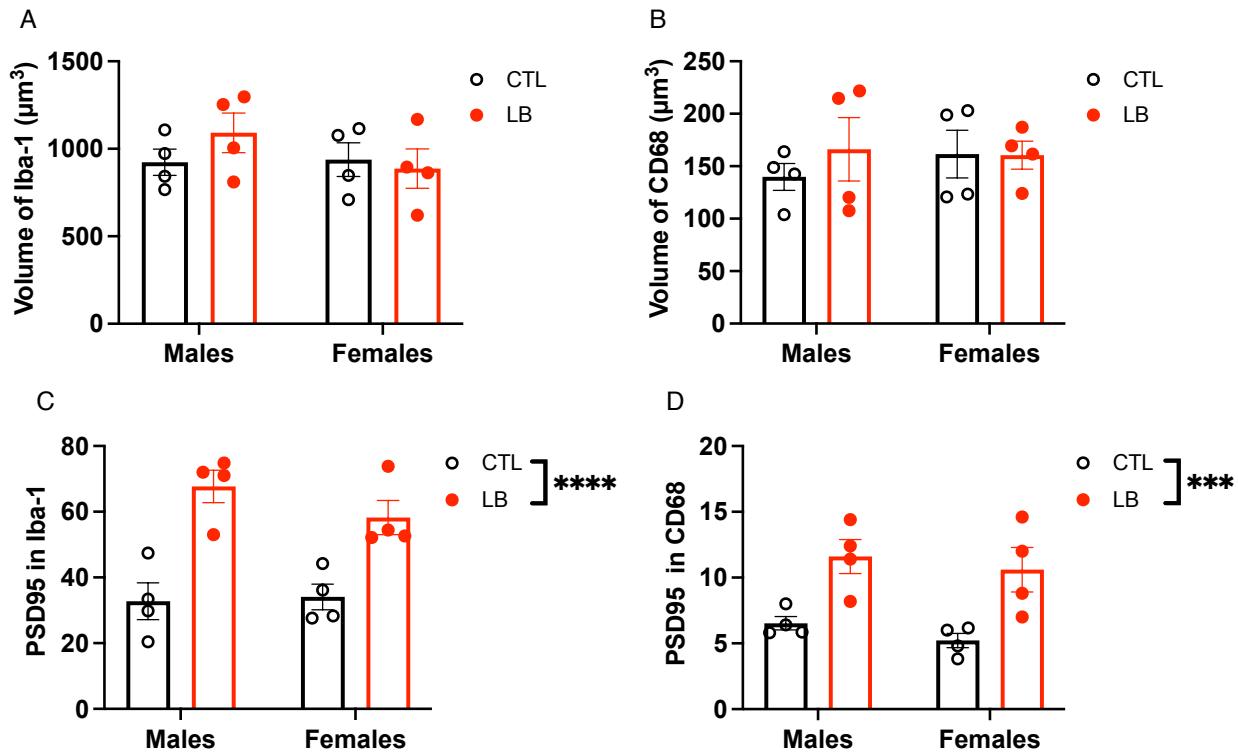
Fig S2. LB Increases Microglial Phagocytic Activity in Adolescent P33 mice. CTL and LB adolescent mice were perfused at P33 to assess microglial volume, CD68 volume, number of PSD95 puncta inside microglia, and number of PSD95 puncta inside CD68. For representative images see figure 2. (A) Microglial volume. Rearing: $F_{(1, 12)} = 0.344$, P= 0.57, Sex: $F_{(1, 12)} = 0.89$, P= 0.36, Interaction: $F_{(1, 12)} = 1.19$, P= 0.29 (B) CD68 phagosome volume inside microglia. Rearing: $F_{(1, 12)} = 0.36$, P= 0.56, Sex: $F_{(1, 12)} = 0.14$, P= 0.71, Interaction: $F_{(1, 12)} = 0.42$, P= 0.53. (C) PSD95 puncta inside microglia. Rearing: $F_{(1, 12)} = 35.54$, P< 0.0001, Sex: $F_{(1, 12)} = 0.67$, P= 0.43, Interaction: $F_{(1, 12)} = 1.18$, P= 0.30 (D). PSD95 puncta inside CD68. Rearing: $F_{(1, 12)} = 21.62$, P= 0.0006, Sex: $F_{(1, 12)} = 1.054$, P= 0.32, Interaction: $F_{(1, 12)} = 0.019$, P= 0.89. Error bars represent mean ± SEM. Two-way ANOVA, ***p< 0.001, ****p< 0.0005.
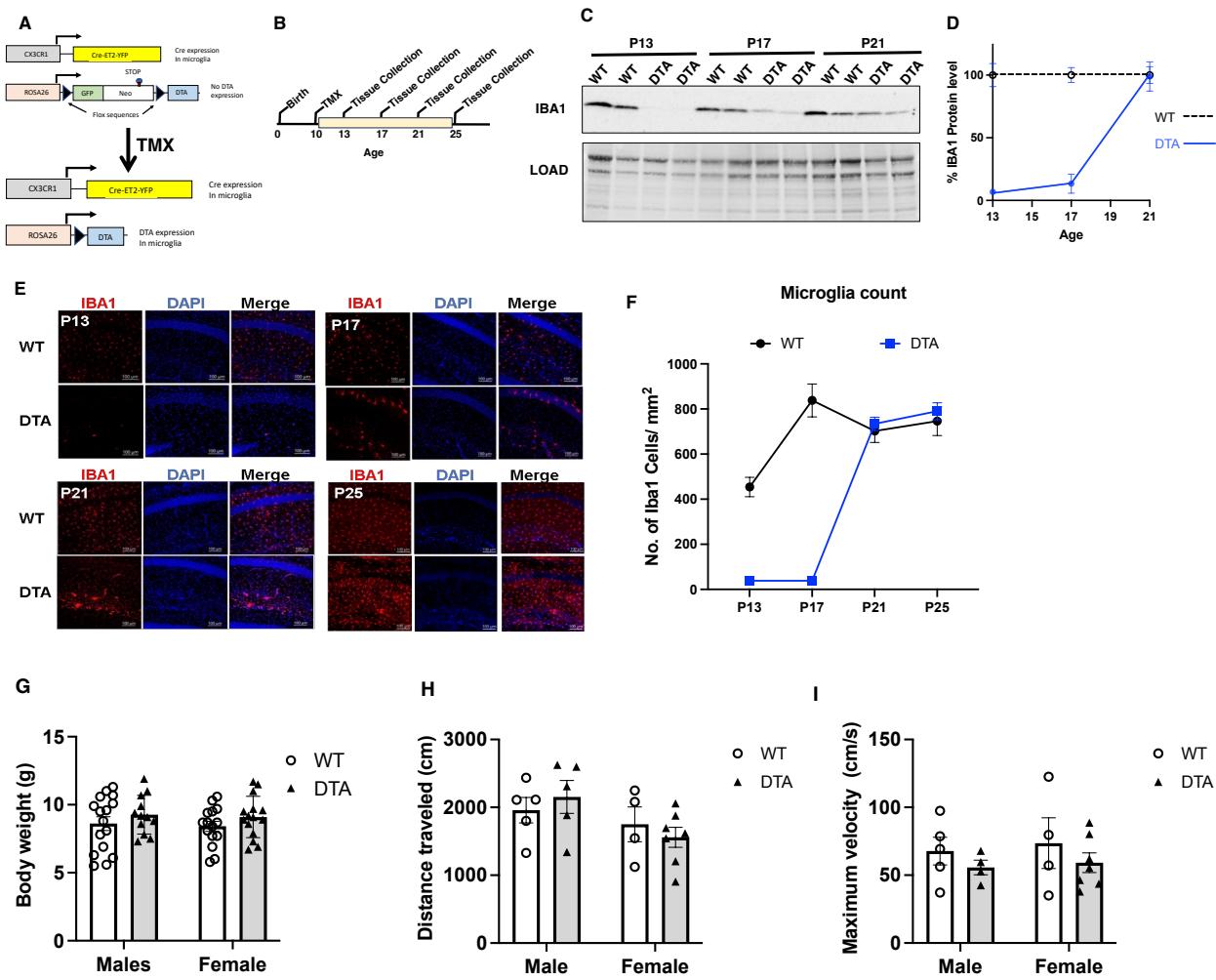
Fig S3. Transient Microglial Ablation During the Second and Third Weeks of Life Does not Impact Weight or Mobility at P17. (A) Schematics of ablation strategy. Tamoxifen (TMX) induces Cre mediated removal of a neomycin-GFP cassette containing a stop codon allowing for the expression of the diphtheria toxin A (DTA) subunit in microglia. (B) Experimental timeline. TMX (30mg/kg) was administered i.p. at P10 and tissue was collected at P13, P17, P21 and P26. (C-D) Western blot and quantification of Iba1 in the hippocampus (N= 5-7 mice per age and genotype, 50% females). (E-F) Confocal images and quantification of the number of Iba1-positive cells in the stratum radiatum (N= 6-8 mice per age and genotype, 50% females). Effects of genotype (WT vs DTA), sex, and their interaction in body weight (G), total distance moved (H) and maximum in the open field test velocity (I). Error bars represent mean ± SEM.
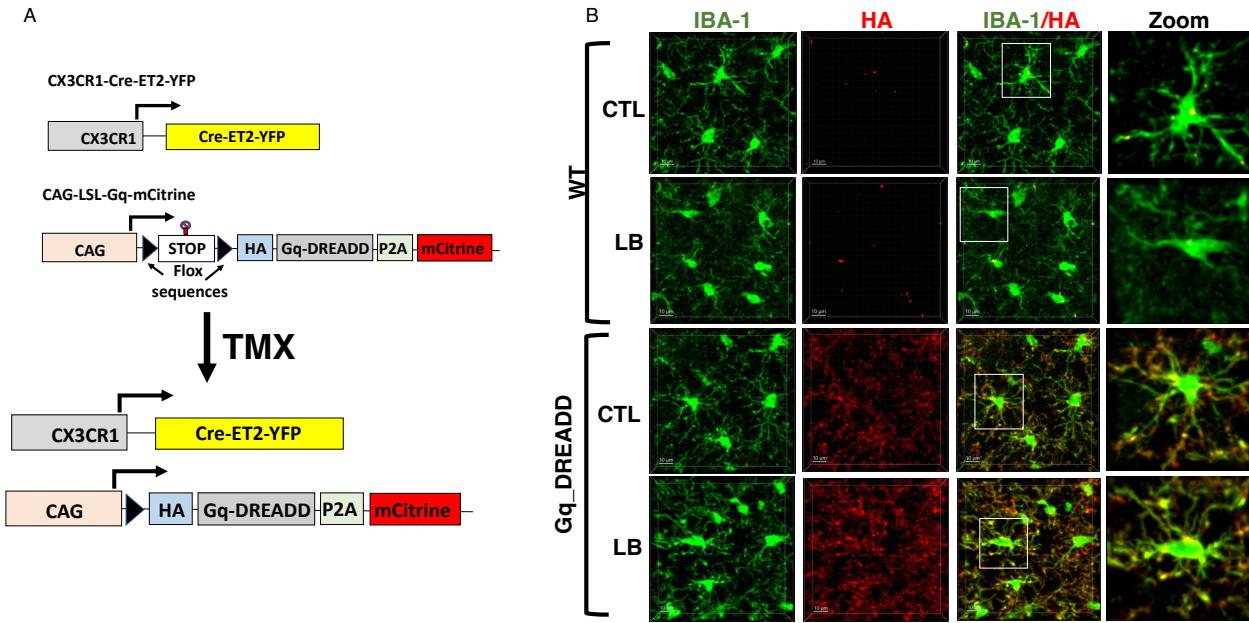
Fig S4- HA-Gq-DREADD expression in P17 Microglia. (A) Schematic illustration of the tamoxifen induced expression of HA-Gq-DREADD in CX3[Cre-ET2]-Gq-DREADD mice. (B) Gq and WT pups were administered tamoxifen i.p. at P10 (30mg/kg), followed by daily CNO injections P13-17 and perfused at P17. Tissue was then stained with anti-HA antibody (1:1000; BioLegend, Cat. #901501) and anti-Iba1 antibodies (1:500; Wako, Cat. #019-19741). HA-Gq-DREADD expression was detected in microglia from Gq but not WT littermates.

5
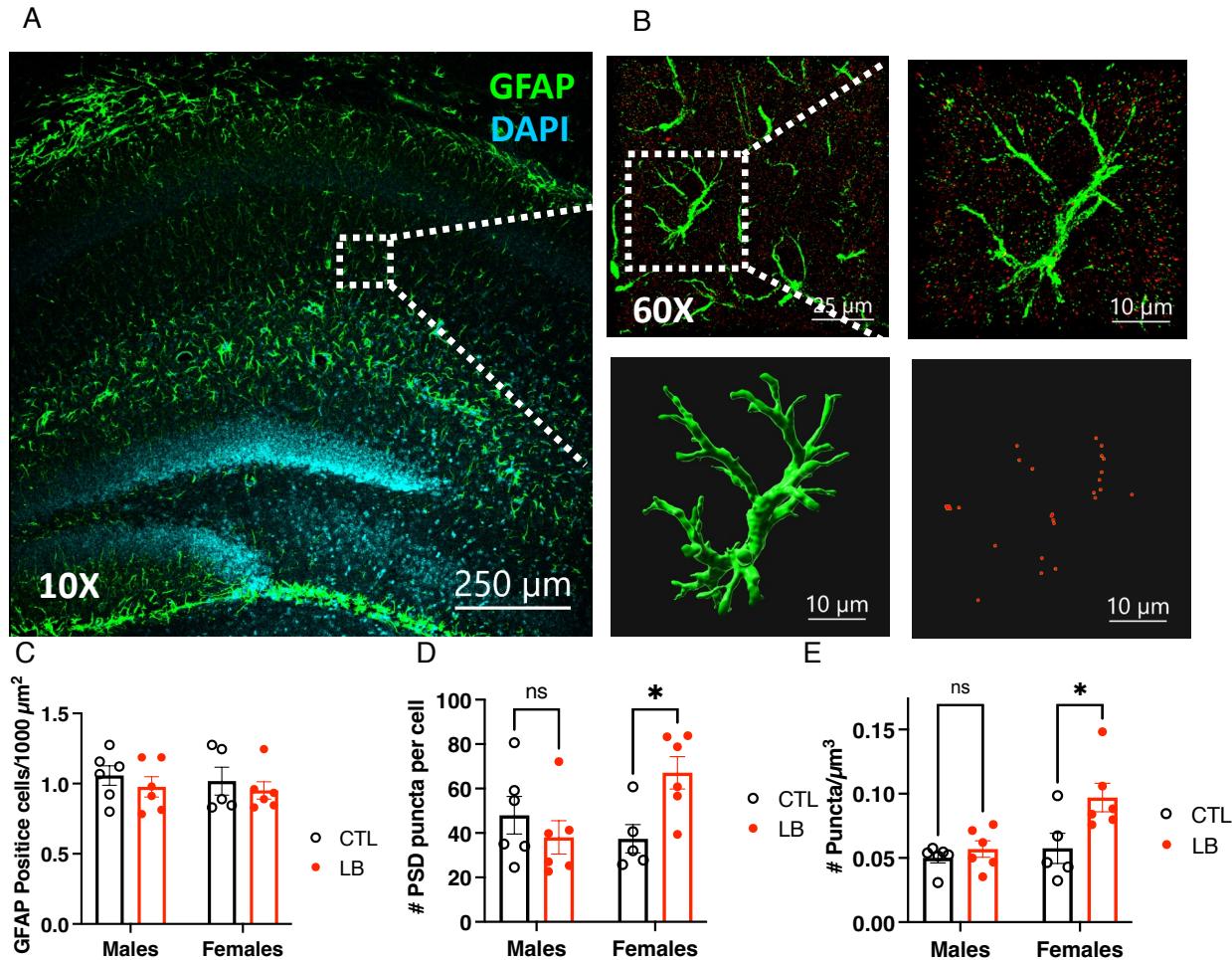
Fig S5- LB Increases Phagocytic Activity in Female Astrocytes Located in the Stratum Radiatum. (A) Low magnification of GFAP-positive cells in the dorsal hippocampus. (B) Higher magnification of GFAP (green) and PSD95 (red) staining and Imaris models of a GFAP-positive astrocyte located in the stratum radiatum and PSD95 puncta inside the cell. (C) Density of GFAP-positive cells in the stratum radiatum. Rearing: $F_{(1, 19)} = 0.95$, P= 0.34, Sex: $F_{(1, 19)} = 0.19$, P= 0.67, Interaction: $F_{(1, 19)} = 0.009$, P= 0.92. (D) Number of PSD95 puncta per GFAP-positive cell, Rearing: $F_{(1, 19)} = 1.694$ P= 0.21, Sex: $F_{(1, 19)} = 1.48$, P= 0.24, Interaction: $F_{(1, 19)} = 6.82$; P= 0.017, Males: P= 0.58, Females: P= 0.028. (E) Density of PSD95 puncta in GFAP-positive astrocytes, Rearing: $F_{(1, 19)} = 7.18$, P= 0.014, Sex: $F_{(1, 19)} = 7.54$; P= 0.013, Interaction: $F_{(1, 19)} = 3.6$, P= 0.073. Males: P= 0.82, Females P= 0.010. Error bars represent mean ± SEM. *p< 0.05.
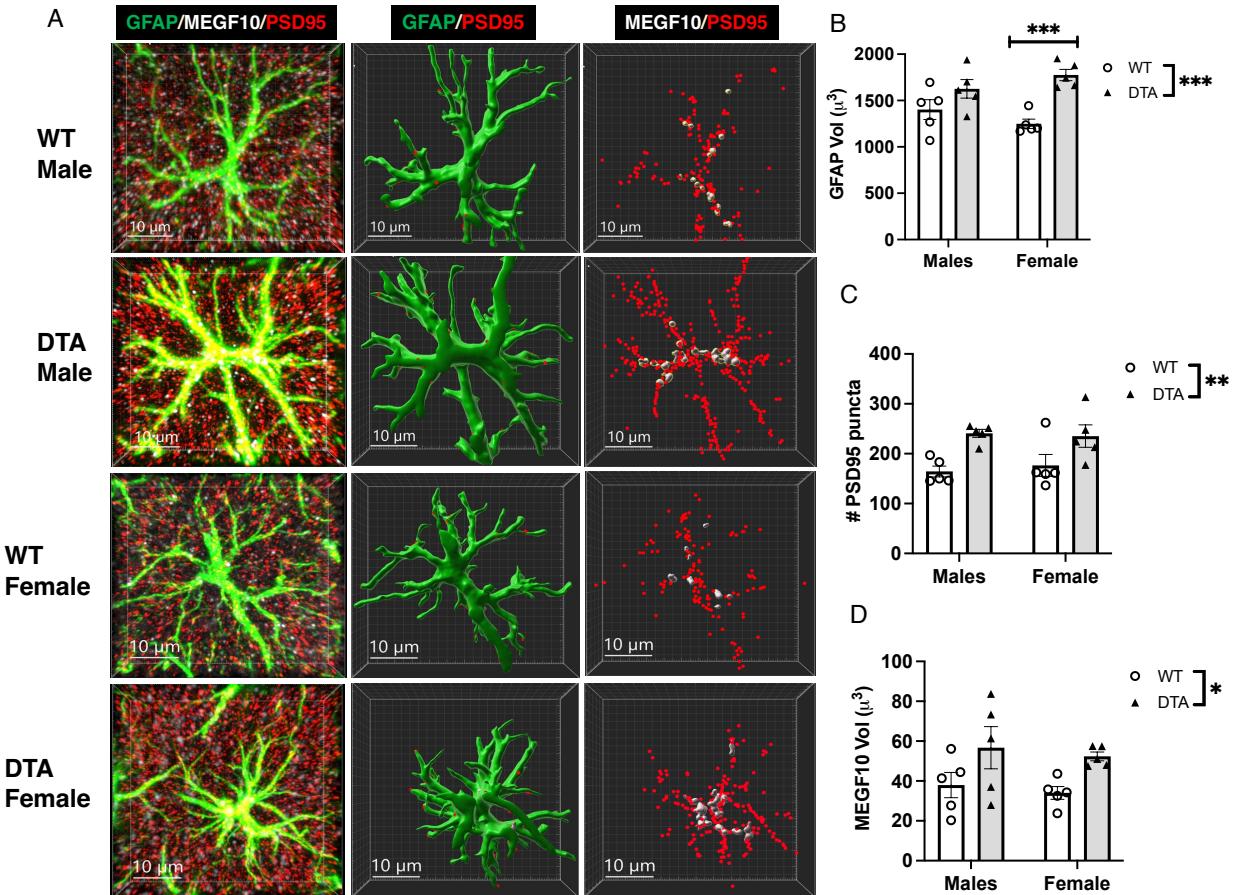
Fig S6. Microglial Ablation Increases PSD95 Puncta and MEGF10 Expression in Normally Developing Male and Female Pups. WT and DTA P10 pups were administered tamoxifen i.p. at P10 and processed at P17 to assess phagocytic activity and MEGF10 levels in GFAP-positive astrocytes located in the stratum radiatum. (A) Representative confocal images and Imaris models. (B) Cell volume, Rearing: $F_{(1, 16)} = 20.34$, P=0.0004, Sex: $F_{(1, 16)} = 0.00037$ P= 0.98, Interaction: $F_{(1, 16)} = 3.33$, P=0.086, Sidak post-hoc, males: P= 0.15, females: P= 0.0008. (C) Number of PSD95 puncta inside GFAP-positive astrocytes, Rearing $F_{(1, 16)} = 15.59$, P=0.0012, Sex: $F_{(1, 16)} = 0.035$, P= 0.85, Interaction: $F_{(1, 16)} = 0.26$, P= 0.62, Sidak post-hoc, males: P= 0.11, females: P= 0.12. (D) MEGF10 staining in astrocytes, Rearing: $F_{(1, 16)} = 8.2$, P= 0.011, Sex: $F_{(1, 16)} = 0.41$, P= 0.53, Interaction: $F_{(1, 16)} = 0.00075$, P= 0.97, Sidak post-hoc, males: P= 0.012, females: P= 0.053. Error bars represent mean ± SEM. *p< 0.05, **p< 0.01, ***p< 0.001.